

Two-Terminal Perovskite-Based Tandem Solar Cells for Energy Conversion and Storage

Tian-Tian Li, Yuan-Bo Yang, Guo-Ran Li, Peng Chen,* and Xue-Ping Gao*

The organic–inorganic hybrid perovskite solar cells present a rapid improvement on power conversion efficiency from 3.8% to 25.5% in the past decades. Owing to the tuneable bandgaps, low-cost, and ease of fabrication, perovskites become ideal candidate materials for fabricating tandem solar cells, especially for efficient and high-voltage monolithic two-terminal devices. In this review, an overview of recent advances in various monolithic perovskite-based tandem solar cells with a focus on the key challenges is provided. Subsequently, the recombination layer materials, construction of wide-bandgap perovskite layer, stability of narrow-bandgap, and current matching principle in tandems are highlighted in order to optimize the output voltage and conversion efficiency of tandem solar cells. Finally, the recent progress is summarized with a focus on potential applications of tandem solar cells for energy conversion and storage, including hydrogen production by water splitting, CO₂ reduction, supercapacitors, and rechargeable batteries, benefiting from the adjustable output voltage of tandem solar cells. It is hoped that this work can offer a feasible strategy to explore more possibilities for fabricating new two-terminal tandem solar cells with high voltage and high conversion efficiency for energy conversion and storage.

Nowadays, the power conversion efficiency (PCE) of single-junction solar cells is almost approaching the theoretical ceiling of 31–33% according to Shockley–Queisser (S-Q) single-junction efficiency limitation.^[2] However, the output voltage of the most efficient single-junction solar cells such as GaAs is about 1 V, which is insufficient for practical application to subsequently drive energy storage/utilization devices. Fortunately, by connecting multiple absorber layers to fabricate the tandem solar cells, the output voltage could be significantly increased as well as the PCE. According to S-Q analysis, the theoretical efficiencies of two-junction and three-junction solar cells could be as high as 42% and 49%, respectively.^[3] Importantly, the output voltage of the tandem solar cells would be nearly doubled or tripled correspondingly. As an example, the open-circuit voltage (V_{OC}) of single line silicon solar cells is only about 0.6 V, which could be increased up to 1.21 V by

stacking CdSe on the top of silicon.^[4] Recently, with the rapid development of high-voltage perovskite solar cells (PSCs), the V_{OC} of the tandem solar cells is remarkably improved. Typically, the highest V_{OC} can reach up to 2.3 V for two-junction tandem solar cells, consisting of two CH₃NH₃PbI₃ (MAPbI₃) subcells.^[5] Though higher voltage could be achieved by adding more junctions, such as 3.21 V in three-junction tandem cells,^[6] 4.227 V for four-junction tandem cells,^[7] 4.40 V for five-junction tandem cells,^[8] and calculated 5.15 V for six-junction tandem cells,^[9] yet the cost and technological requirements would increase exponentially. It is noted that although solar modules with simple serial connected design can also provide high voltage, the light management is still the same as single-junction cells, which could never beyond S-Q limitation. Tandem solar cells could provide a possibility for breaking physical limitation of traditional single-junction solar cells. Besides, tandem solar cells could also be basic unit for solar modules to obtain higher efficiency.

As shown in **Figure 1**, tandem solar cells could deliver high PCE and V_{OC} by segmented light adsorption. The PCE of solar cells is determined mainly by two processes: light absorption and carriers separation/collection. Usually, short-circuit current density (J_{SC}) would be lower than theory limit because of incomplete light absorption and sluggish collection of generated carriers, whereas a reduced V_{OC} or fill factor (FF) reflects

1. Introduction

With the development of human society and enhanced living standard, the meagre energy reserves of fossil fuels can hardly achieve long-term sustainability. Correspondingly, the resulting environmental pollution by fossil fuels is also nonnegligible issue. It is thus critical to develop new technologies of utilizing ever-lasting and clean energy sources like solar irradiation. Solar energy is so enormous that 0.1% of the solar irradiation reaches the earth can cover the consumption of human society.^[1] Meanwhile, the electrical energy is the foundation of modern industries and daily life. Therefore, advanced photovoltaics technologies are highly important for efficiently converting solar energy to electrical energy.

T.-T. Li, Y.-B. Yang, Prof. G.-R. Li, Dr. P. Chen, Prof. X.-P. Gao
Institute of New Energy Material Chemistry
School of Materials Science and Engineering
Nankai University
Tianjin 300350, China
E-mail: chenpengnk@nankai.edu.cn; xpgao@nankai.edu.cn

 The ORCID identification number(s) for the author(s) of this article can be found under <https://doi.org/10.1002/sml.202006145>.

DOI: 10.1002/sml.202006145

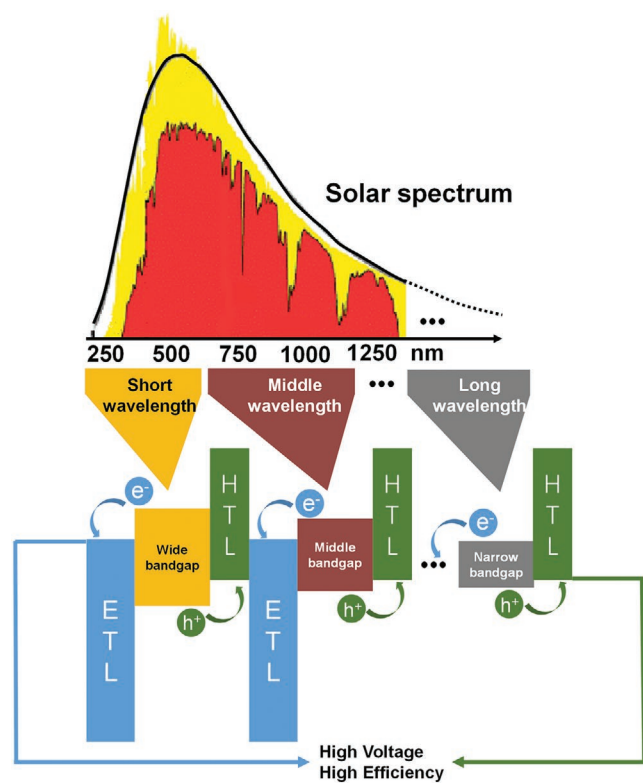


Figure 1. Schematic diagram of tandem solar cells achieving high output voltage and efficiency by segmented light adsorption.

carriers recombination process within bulk or on the interface. Tandem cells could effectively broaden the light absorption range by involving more subcells. Each subcell would convert a certain range of solar spectrum, which is beneficial to fully adsorption of solar spectrum, as well as the increase of output voltage by several-folds. However, owing to the high cost, two-junction tandem solar cells are the most feasible photovoltaics technologies from a practical perspective, and researchers are devoted mainly to improve the efficiency and voltage of this type of solar cells. In this review, we will focus on two-junction tandems and keeping an open mind on promising applications of multiple junction tandem solar cells.

There are two types of two-junction tandem solar cells based on the architectures: mechanically stacked four-terminal (4T) tandem configurations, and integrated two-terminal (2T) tandem configurations. 4T tandem devices, with two individual solar cells connected by external wires, are not preferred due to the extra energy losses from substrates, transparent conductive oxides (TCO), and interconnect layers. As a comparison, 2T tandem devices are fabricated layer-by-layer in a single integrated structure by two subcells, and thus this structure enables less energy losses in theory. Herein, more accurate optical and electrical matching should be optimized in 2T structure, aiming at entire absorption of solar spectrum and identical current matching between the subcells. In particular, an interlayer with low electrical and optical losses is required to facilitate the flow of photogenerated carriers between the two subcells, which in turn retards the development of 2T devices. Fortunately, owing to further improved technologies on optimal bandgap configurations^[10]

and transparent buffer layers,^[11] 2T tandem cells could realize high efficiency and unprecedented high voltage, especially when combined with advanced high-voltage PSCs.

PSC is a rising star of solar cells, which is attributed to the rocketing PCE from 3.8%^[12] to 25.5%,^[13] and the V_{OC} reaching up to 1.2 V, making PSCs extremely attractive. As the most typical perovskite component, MAPbI₃ has a suitable bandgap of 1.55 eV, which not only enables full absorption for the visible solar spectrum, but covers a broad spectral range extending to the near-infrared region up to 800 nm.^[14] Along with excellent optical properties, PSCs own high absorption coefficient ($\approx 10^5 \text{ cm}^{-1}$),^[15] long ambipolar diffusion length exceeding 1 μm , and high charge carrier mobility ($24 \pm 7 \text{ cm}^2 \text{ V}^{-1} \text{ s}^{-1}$ for electrons and $105 \pm 5 \text{ cm}^2 \text{ V}^{-1} \text{ s}^{-1}$ for holes^[16]), leading to efficient charge extraction. Moreover, the substitution of structure elements allows widely tunable bandgaps between 1.17 and 3.10 eV.^[14a,17] For example, perovskite materials have the general formula of ABX₃, in which A, B, and X represent monovalent cations (CH₃NH₃⁺ (MA⁺), HC(NH₂)₂⁺ (FA⁺), and Cs⁺), divalent cations (Pb²⁺ and Sn²⁺), and monovalent halide anions (I⁻, Br⁻, and Cl⁻), respectively. The bandgap of perovskite materials can be tuned by altering elements on A, B, and X sites to achieve various light absorption ranges, thus balancing the PCE and V_{OC} . Such tunable bandgap range and high efficiency makes perovskite material suitable as both the top and bottom cell in one unit of tandem solar cells, resulting in improved PCE and V_{OC} for 2T tandem devices. Consequently, PCE and V_{OC} of 2T tandem cells are significantly boosted by pairing PSCs with narrow-bandgap silicon (Si), copper indium gallium selenide (CIGS), or organic photovoltaic (OPV) bottom cells or directly using two complementary bandgap perovskite absorbers. **Figure 2** shows the efficiency evolution of four types of 2T perovskite-based tandem solar cells (2T-PBTSCs) including 2T perovskite/perovskite tandem solar cells (2T-PSC/PSC), 2T perovskite/silicon tandem solar cells (2T-PSC/Si), 2T perovskite/CIGS tandem solar cells (2T-PSC/CIGS), and 2T perovskite/organic tandem solar cells (2T-PSC/OPV).

In this review, recent advances in the field of 2T-PBTSCs are summarized, with a focus on the bandgap matching and

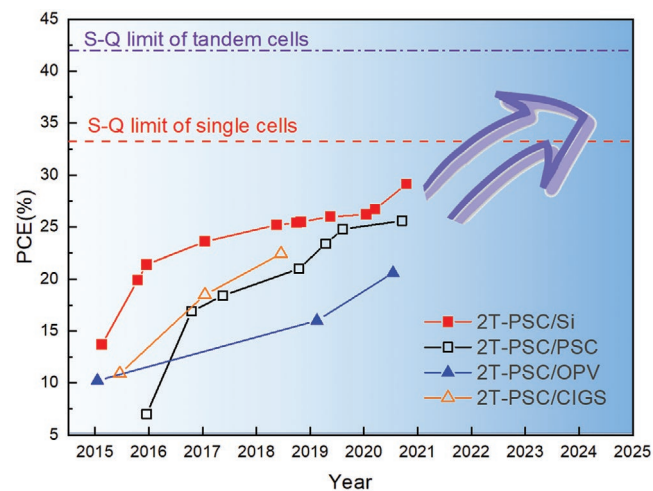


Figure 2. PCE evolution of tandem solar cells involving PSCs: 2T-PSC/PSC, 2T-PSC/Si, 2T-PSC/OPV, and 2T-PSC/CIGS tandem solar cells.

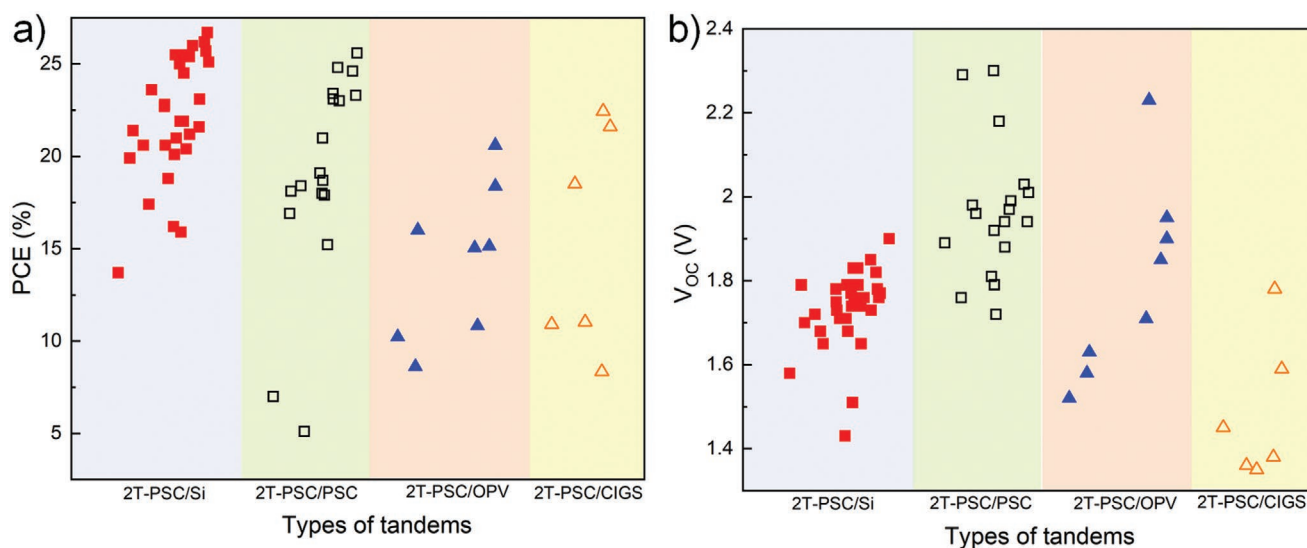


Figure 3. a) PCE and b) V_{oc} evolution of 2T-PSC/PSC, 2T-PSC/Si, 2T-PSC/OPV, and 2T-PSC/CIGS.

charge recombination layer (CRL). Particularly, the output voltage development of 2T tandem cells is discussed in order to fulfill the requirement of energy conversion and storage. Finally, some potential applications of 2T-PBTSCs are presented by referencing the integration of single-junction solar cells with energy storage/utilization devices. It is believed that 2T tandem architectures are still the most desirable and challenging configuration, which satisfy perfectly the high voltage for practical demands and relatively acceptable cost. In addition, the integrated systems with various energy storage/utilization devices facilitate fundamentally the utilization of clean energy.

2. 2T-PBTSCs

The single-junction PSCs have achieved tremendous development in recent years, thus driving 2T-PBTSCs for comparative ideal performance. With tunable bandgap, the perovskite absorber can act as active material in both top subcell and bottom subcell to construct 2T tandem solar cells.

In 2T tandem structure, the currents through top and bottom subcells need to be equal, which requires well-complementary bandgaps and matched absorber thickness. As discussed above, there are two key processes that affect the performance of solar cells: light absorption and carriers separation/collection. Specifically, in 2T tandem structure, two subcells must provide balanced carriers density of electrons and holes, which would be neutralized within the CRL. In this way, bandgap structure of two subcells must be well-designed for complementary light absorption. Meanwhile, the absorber thickness must be adjusted for suitable light and electrical matching. In addition, the CRL plays a crucial role to connected subcells monolithically, for which higher transmittance and less electrical losses are always the target to be pursued. Along with the promotion of single-PSC with wider and narrower bandgaps and the development of the charge recombination layer, the V_{oc} of tandem devices is enhanced to almost double of single-junction solar cell, the PCE of 2T-PBTSCs is increased progressively

meanwhile, as shown in **Figure 3a**. Herein, four types of 2T tandem structures hold various advantages and disadvantages. 2T-PSC/Si and 2T-PSC/CIGS have the feature of high PCE, and ease for commercialization, but relatively high cost and lack of flexibility. As contrast, 2T-PSC/OPV and 2T-PSC/PSC show a great potential for future development in PCE and particular superiority of lightweight, convenient, and flexible devices. Noteworthy, 2T-PSC/PSC devices hold remarkably high V_{oc} (**Figure 3b**), which is credited to the desired bandgap matching. Although J_{sc} also plays an important role in solar cells performance, the structure and building-principle of tandem solar cells is segmented absorption of solar spectrum, which would reduce J_{sc} and improve V_{oc} . Therefore, in this review, we mainly focus on the advantage of high V_{oc} and the potential application derived from high V_{oc} based on the potential application in integrated devices for energy conversion and storage.

2.1. 2T Monolithic Perovskite/Silicon Tandem Solar Cells

At present, crystalline Si solar cell is the maturest photovoltaic technology which still dominates most photovoltaic market. The champion efficiency of Si photovoltaic is 26.6%,^[51] very close to the theoretical efficiency of 29.4%.^[52] At the same time, the V_{oc} of the Si solar cell is only 0.5–0.6 V, which is hard to satisfy the demand of the high voltage in practical applications. Constructing a tandem device with wide-bandgap PSC is a promising approach to break those limitations on the output voltage. **Figure 4** shows the PCE evolution of four types of Si tandem solar cells, and detailed photovoltaic parameters of 2T-PSC/Si are summarized in **Table 1**.

The first tandem device was developed by Mailoa and co-workers,^[18] as shown in **Figure 5a–d**. MAPbI₃ with 1.61 eV bandgap is employed on top subcell, which is assembled with an n-type Si solar cell as the bottom subcell. In order to process the perovskite layer, the top surface of crystalline silicon (c-Si) subcell should be polished carefully. A silicon-based n⁺/p⁺ interband tunnel junction is a key enabler for facilitating the

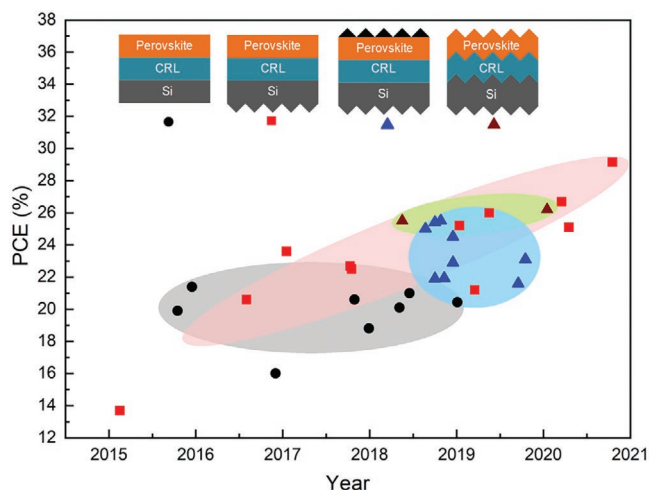


Figure 4. PCE evolution of four types of 2T-PSC/Si classified by the surface states (polished or textured).

carrier recombination effectively. Between the heavily doped n^{++} hydrogenated amorphous silicon (α -Si:H) and p^{++} emitter, the intrinsic c -Si layer is inserted, which facilitates the inter diffusion of dopant species and retained the tunnel junction conductivity. In addition, the light is irradiated from the metal back electrode, thus the perovskite electrode should be conductive and transparent. A mechanical transfer method^[53] is adopted to fabricate silver nanowires (AgNWs) electrode, which has a sheet resistance of $9 \Omega \square^{-1}$ and a peak transmission of 89.5%. Accordingly, a stabilized PCE of 13.7% was performed in the first perovskite-silicon integrated tandem solar cell. Noteworthy, the V_{OC} is obtained as high as 1.65 V, which is almost the sum of the perovskite and filtered Si's V_{OC} , demonstrating the superb potential of 2T-PSC/Si.

The α -Si:H/ c -Si heterojunction (SHJ) can reach higher V_{OC} up to 750 mV as compared to diffused homojunction cells with a V_{OC} around 700 mV, because high-quality intrinsic (i) α -Si:H layer can passivate the surface dangling bonds of c -Si.^[54] Correspondingly, a monolithic perovskite/SHJ tandem cell is developed,^[19] which formed by a (p,i) α -Si:H/(n)c-Si heterojunction bottom subcell and a perovskite with $FA_{0.83}MA_{0.17}Pb(I_{0.83}Br_{0.17})_3$ as top subcell (Figure 5e–h). To avoid the transfer and effuse of hydrogen at $\approx 200^\circ C$, a planar and low-temperature SnO_2 is implemented as the electron transport layer (ETL) to replace the high-temperature mesoporous and compact TiO_2 . By introducing high V_{OC} SHJ to 2T-PSC/Si, the device presents the high V_{OC} of 1.78 V and stabilized PCE of 18.1%. However, the performance of the tandem device is limited by the photocurrent generated in the Si bottom subcell. Subsequently, to optimize the light management, the thicknesses of indium zinc oxide (IZO) CRL and the hole transport layer (HTL) are researched by experiments and optical simulations.^[20] The V_{OC} of 1.69 V, and PCE of 21.2% can be obtained, due to the increased J_{SC} of 15.9 mA cm^{-2} .

Nevertheless, double-side polished Si bottom cells show slow spectral response in the SHJ rear side, causing reflection losses and inferior performance. Thus, it is rational to replace the polished Si substrate with a textured Si to improve the light-trapping and J_{SC} of the bottom cell.^[55] Owing to the increased

optical path length, the light-trapping and near-infrared spectral response is enhanced, hence increasing J_{SC} . A monolithic perovskite/SHJ tandem solar cell with rear-side textured Si is displayed in Figure 5i–l, which shows an enhanced quantum efficiency in the near-infrared region. After texturing the Si rear side, the bottom subcell current density is enhanced by 0.77 mA cm^{-2} , and the whole device current density is increased from $16.1^{[20]}$ to 16.4 mA cm^{-2} .^[21] Accordingly, the PCE increases from 19.2% to 20.5%, and a higher V_{OC} of 1.72 V is obtained. Generally, the instability of the PSC is the bottleneck of 2T-PSC/Si system, especially the severe phase separation of the wide-bandgap perovskite subcell under illumination. Recently, Kim et al. reported a 2D–3D mixed strategy to stabilize PSC through phenethylammonium thiocyanate (PEASCN) and phenethylammonium iodine (PEAI).^[48] The PEA^+ could passivate the surface and grain boundaries by preferentially inducing 2D phase. The high-quality perovskite subcell is then obtained as demonstrated by the microsecond long lifetime and high mobility. When combined with a backside-texture Si bottom cell, the tandem device presents 26.7% PCE with a V_{OC} of 1.756 V and negligible hysteresis.

With a similar consideration, a textured light management foil on the front-side of the tandem solar cell can be employed to reduce reflection and enhance light trapping at the textured light management (LM) foil/air interface,^[34] as shown in Figure 5m–p. By efficient light management, the device with LM foil can reach a remarkable PCE of 25.5%, the highest reported efficiency for the 2T-PSC/Si, while a high V_{OC} of 1.76 V is maintained.

Generally, the front surface of Si tends to be smooth to achieve direct deposition of perovskite on Si subcell, leading to inevitable reflection losses and nonideal light trapping. If a fully textured Si wafer can be applied to monolithic perovskite/SHJ tandem cells, the performance could be further improved. In this way, an effective structure for 2T-PSC/Si is considered by comparing the optic and photovoltaic properties of textured and flat surfaces of Si/perovskite.^[56] Due to the enhancement of light trapping, the textured device could reduce the reflectance of the Si surface as compared with the flat Si surface (from 2.7% to 0.8%), resulting in the increase in average incident photon to current conversion efficiency values (from 83.0% to 88.0%) and J_{SC} (from 13.7 to 14.8 mA cm^{-2}). However, the spin-coating deposition of perovskite subcell is limited by the rough Si surface because the texture size of Si is larger than the thickness of the perovskite layer, which is about 5–10 μm and 200–500 nm, respectively. A deposition method for preparing conformal perovskite absorber layers on textured SHJ bottom cells is explored as indicated in Figure 5q–t.^[30] The conformal perovskite film is produced by a hybrid two-step method including sequential co-deposition and spin coating. A nanocrystalline Si recombination junction is used between two subcells, providing a high resilience to shunts. As a result, the introduction of a frontal texture reduces the overall reflectivity to below 2% in the range $\lambda = 360$ –1000 nm, and reduce the current loss from 3.14 mA cm^{-2} to an equivalent integrated photocurrent value of 1.64 mA cm^{-2} in the wavelength range of $\lambda = 360$ –1200 nm, as compared to the rear-side texture monolithic cell. The fully textured SHJ as bottom subcell allows the J_{SC} and V_{OC} of a 2T-PSC/Si tandem device to reach 19.5 mA cm^{-2} and 1.79 V,

Table 1. Summary of the 2T monolithic perovskite/silicon tandem solar cells.

Publish date	Top cell	E_g [eV]	Bottom cell	RCL	V_{oc} [V]	J_{sc} [mA cm ⁻²]	FF	PCE [%]	Steady PCE [%]	Area [cm ²]	Ref.
2015.02	MAPbI ₃	1.61	nc-Si	n ⁺⁺ Si p ⁺⁺ Si	1.58	11.5	0.75	13.7	13.7	1	[18]
2015.10	FA _{0.83} MA _{0.17} Pb(I _{0.83} Br _{0.17}) ₃	–	SHJ	ITO	1.79	14.0	0.80	19.9	18.1	0.16	[19]
2015.12	MAPbI ₃	1.55	SHJ	IZO	1.70	15.9	0.80	21.4	21.2	0.17	[20]
					1.70	16.1	0.71	19.5	19.2	1.22	
2016.07	MAPbI ₃	1.55	SHJ	IZO	1.72	16.4	0.73	20.6	20.5	1.43	[21]
2016.12	MAPbI ₃	1.55	nc-Si	ZTO	1.64	15.3	0.65	16.3	16.0	1.43	[22]
					1.68	15.3	0.68	17.4	16.4	0.25	
2017.02	Cs _{0.17} FA _{0.83} Pb(Br _{0.17} I _{0.83}) ₃	1.63	SHJ	ITO	1.65	18.1	0.79	23.6	23.6	1	[23]
2017.10	Cs _{0.07} Rb _{0.03} FA _{0.765} MA _{0.135} PbI _{2.55} Br _{0.45}	1.62	nc-Si	ITO	1.75	17.6	0.74	22.8	22.5	1	[24]
2017.10	Cs _{0.19} FA _{0.81} Pb(I _{0.78} Br _{0.22}) ₃	1.63	SHJ	nc-Si:H	1.75	16.8	0.78	22.7	22.0	0.25	[25]
					1.78	16.5	0.74	21.8	21.2	1.43	
					1.77	16.5	0.65	19.1	18.0	12.96	
2017.10	MA _{0.37} FA _{0.48} Cs _{0.15} PbI _{2.01} Br _{0.99}	1.69	SHJ	ITO	1.70	15.3	0.79	20.6	18.0	0.03	[26]
2017.12	FA _{0.75} MA _{0.25} Pb(I _{0.76} Br _{0.24}) ₃	–	SHJ	ITO	1.71	15.49	0.71	18.8	–	0.13	[27]
					1.67	14.74	0.67	16.5	–	1	
2018.05	–	–	SHJ	ITO	1.71	15.87	0.74	20.1	–	0.53	[28]
2018.06	MAPbI ₃	1.58	n-Si	SnO ₂	1.68	16.1	0.78	21.0	20.5	4	[29]
					1.66	15.6	0.68	17.6	17.1	16	
2018.06	Cs _x FA _{1-x} Pb(I,Br) ₃	1.6	SHJ	ITO	1.79	19.5	0.73	25.5	25.2	1.42	[30]
2018.07	Cs _{0.17} FA _{0.83} Pb(Br _{0.17} I _{0.83}) ₃	–	pc-Si	ITO	1.43	15.3	0.75	16.2	16	1	[31]
2018.08	FA _{0.83} MA _{0.17} Pb(Br _{0.17} I _{0.83}) ₃	1.59	nc-Si	SnO ₂	1.74	16.2	0.78	21.9	21.8	16	[32]
2018.08	FA _{0.75} Cs _{0.25} Pb(I _{0.8} Br _{0.2}) ₃	1.68	SHJ	ITO	1.77	18.4	0.77	25.0	–	1	[33]
2018.10	Cs _{0.05} (MA _{0.17} FA _{0.83})Pb _{1.1} (I _{0.83} Br _{0.17}) ₃	1.63	SHJ	ITO	1.76	18.5	0.79	25.5	–	0.77	[34]
2018.11	Cs _{0.1} (FA _{0.75} MA _{0.25}) _{0.9} Pb(I _{0.78} Br _{0.22}) ₃	1.67	SHJ	ITO	1.75	16.89	0.74	21.9	–	0.13	[35]
2018.12	Cs _{0.05} Rb _{0.05} FA _{0.765} MA _{0.135} PbI _{2.55} Br _{0.45}	1.63	SHJ	ITO	1.76	17.8	0.78	24.5	24.1	1	[36]
			nc-Si		1.70	17.2	0.78	22.9	22.9	1	
2019.01	Cs _{0.1} (FA _{0.75} MA _{0.25}) _{0.9} Pb(I _{0.78} Br _{0.22}) ₃	1.67	SHJ	ITO	1.83	15.95	0.70	20.4	–	0.13	[37]
2019.01	Cs _{0.15} (FA _{0.83} MA _{0.17}) _{0.85} Pb(I _{0.8} Br _{0.2}) ₃	1.64	SHJ	ITO	1.80	17.8	0.79	25.4	–	–	[38]
	Cs _{0.15} (FA _{0.83} MA _{0.17}) _{0.85} Pb(I _{0.7} Br _{0.3}) ₃	1.70			1.83	16.4	0.75	22.4			
	Cs _{0.15} (FA _{0.83} MA _{0.17}) _{0.85} Pb(I _{0.75} Br _{0.25}) ₃	1.68			1.81	17.1	0.79	24.5			
	Cs _{0.15} (FA _{0.83} MA _{0.17}) _{0.85} Pb(I _{0.85} Br _{0.15}) ₃	1.62			1.77	17.4	0.78	24.1			
2019.02	Cs _{0.05} (FA _{0.83} MA _{0.17}) _{0.95} Pb(I _{0.82} Br _{0.18}) ₃	1.63	SHJ	ITO	1.79	19.02	0.75	25.4	25.2	1	[39]
2019.03	FA _{0.8} MA _{0.2} PbBr _{0.6} I _{2.4}	1.64	pc-Si	ITO	1.65	16.12	0.80	21.2	21.1	0.135	[40]
2019.03	FACsPbI ₃ Br	–	pc-Si	nc-Si(p):H	1.74	19.5	0.75	25.4	25.1	1.42	[41]
2019.05	Cs _{0.05} (MA _{0.17} FA _{0.83})Pb(I _{0.83} Br _{0.17}) ₃	–	SHJ	ITO	1.76	19.2	0.77	26.0	26.0	0.77	[42]
2019.09	FA _{0.75} Cs _{0.25} Pb(I _{0.8} Br _{0.2}) ₃	1.7	SHJ	ITO	1.85	15.2	0.77	21.6	21.1	0.25	[43]
2019.10	FAMAPbI _{3-x} Br _x	1.61	nc-Si	SnO ₂	1.73	16.5	0.81	23.1	23.0	4.00	[44]
2020.01	Cs _{0.1} MA _{0.9} Pb(I _{0.9} Br _{0.1}) ₃	–	SHJ	ITO	1.82	19.2	0.75	26.2	26.1	–	[45]
2020.02	(Cs _{0.06} FA _{0.78} MA _{0.16})Pb(Br _{0.17} I _{0.83}) ₃	1.64	SHJ	ITO	1.80	18.81	0.77	26.3	25.9	1.43	[46]
2020.02	Cs _{0.05} MA _{0.15} FA _{0.8} PbI _{2.25} Br _{0.75}	1.68	SHJ	InO _x	1.78	15.87	0.75	25.7	25.7	0.832	[47]
2020.03	(FA _{0.65} MA _{0.2} Cs _{0.15})Pb(I _{0.8} Br _{0.2}) ₃	1.68	SHJ	ITO	1.76	19.2	0.79	26.7	26.7	0.188	[48]
2020.04	FA _{0.75} Cs _{0.25} Pb(I _{0.8} Br _{0.2}) ₃	1.68	SHJ	ITO	1.77	17.7	0.80	25.1	25.1	0.25	[49]
2020.10	Cs _{0.05} (FA _{0.77} MA _{0.23}) _{0.95} Pb(I _{0.77} Br _{0.23}) ₃	1.68	SHJ	ITO	1.90	19.3	0.80	29.1	29.1	1.064	[50]

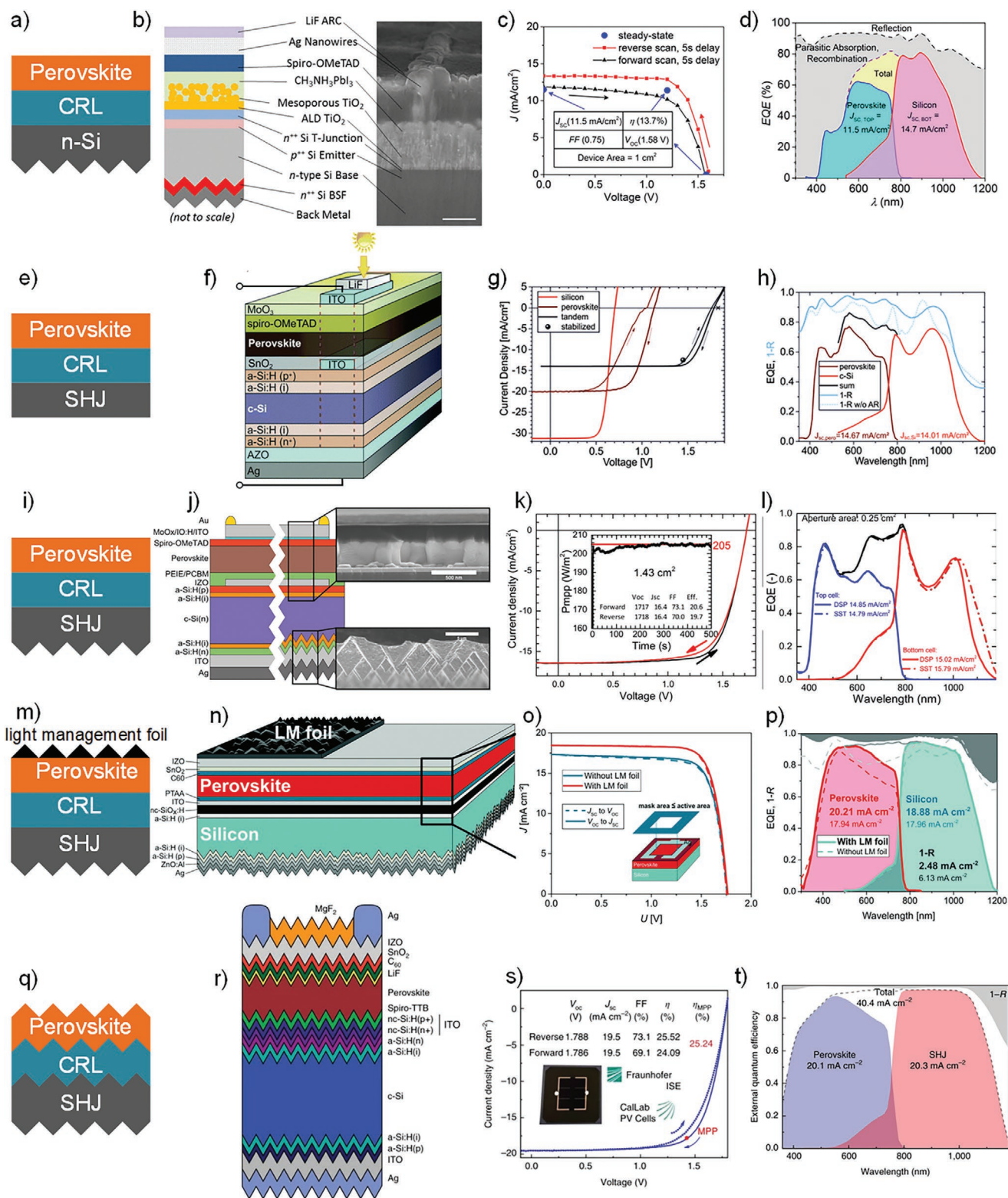


Figure 5. Typical device structure and performance of 2T-PSC/Si. a–d) Tandem solar cell with an n-type Si base. Reproduced with permission.^[18] Copyright 2015, AIP Publishing LLC. e–h) The Si heterojunction/perovskite tandem solar cell. Reproduced with permission.^[19] Copyright 2016, The Royal Society of Chemistry. i–l) Tandem solar cell-based rear-side textured Si. Reproduced with permission.^[21] Copyright 2016, American Chemical Society. m–p) Tandem solar cell-based textured light management foil on the front-side of a tandem solar cell. Reproduced with permission.^[34] Copyright 2018, The Royal Society of Chemistry. q–t) Fully textured monolithic perovskite/SHJ tandem solar cell. Reproduced with permission.^[30] Copyright 2018, Springer Nature.

thus a steady-state efficiency of 25.2% is obtained. Despite that evaporation process demands precise and complex control over the deposition rates of components, this technology is still widely used for preparing PSCs subcell on textured Si pyramids bottom cells. On the rough surface of Si, solution prepared PSC layer could hardly cover Si pyramids, resulting in shunt paths and inefficient charge collection. To solve the coverage problem, Hou et al. demonstrate a solution by increasing the perovskite thickness.^[47] The diffusion length in the thick perovskite film can be increased by anchoring a self-limiting passivant (1-butane-1-thiol) on the perovskite surfaces. The as-prepared 2T-PSC/Si presents a stabilized PCE of 25.7% with V_{OC} of 1.793 V. Besides the sequential deposition of PSC layer on Si cell, a mechanically stacked method to fabricate 2T-PSC/Si is also developed.^[46] The two subcells are independently fabricated and then coupled by contacting the back electrode of the perovskite top cell with the texturized and metalized front contact of the silicon bottom cell. The superior electrical contact enables a high PCE of 26.3% on an active area of 1.43 cm².

Along with several researches on Si part, the J_{SC} of perovskite subcells is also explored to ensure better matching. The theoretical investigation for MAPbI₃-based 2T-PSC/Si by varying thickness of top perovskite layer from 50 to 1000 nm is an important attempt.^[57] In particular, a nearly matched optical absorption and current among the subcells are necessary for better light and carrier management thus achieving high efficiency. The champion efficiency can reach 20.92%, 1.47 times higher than perovskite cell. Furthermore, the methods to adjust bandgap of perovskite have been developed, so that 2T-PSC/Si could present higher performance.^[58] After extensive simulation of various bandgaps of perovskite materials, the optimum performance is obtained when the bandgap of perovskite layer is 1.73 eV, corresponding to an absorption onset of 715 nm. The optimized compatibility between the top and bottom cells is achieved, in which 1748 and 1747 mA cm⁻² can be generated in the perovskite and silicon subcells, respectively.^[59] Considering that there are numerous factors could affect the actual performance of solar cells, this value (1.73 eV) might need further adjustment during experiments. Note that, by replacing the traditional MAPbI₃ with the latest FA⁺ and Cs⁺ hybrid perovskite top cell^[60] in rear-side textured 2T-PSC/Si, and introducing a bilayer of SnO₂ and ZTO as a window layer,^[23] an optimized device presents a high efficiency of 23.6% with V_{OC} of 1.65 V and negligible hysteresis.

The CRL is the critical link in 2T tandem solar cells, so the related researches are still keep moving. p⁺/n⁺ hydrogenated nanocrystalline silicon is widely used in III–V semiconductor and thin-film Si tandem solar cells, which could reduce parasitic absorption and reflection losses at the interface between the subcells, and increase the bottom cell current density.^[61] As a result, the device presents a high efficiency of up to 22.7% on an area of 0.25 cm², and shows up to 1.78 V for the 1.43 cm² large area. To further reduce the reflection losses at the internal junction, the interlayer consisting of nanocrystalline Si oxide is introduced.^[39] The optical properties of the layer can be tuned over a wide range by varying the oxygen content, leading a significantly increased bottom-cell current density, which is driven by better light in-coupling into the bottom cell. As a result, the optimized tandem cells deliver over 19 mA cm⁻² J_{SC} and stabilized PCE of 25.2%.

In addition to solution and vacuum deposition method, slot-die-coating and blade-coating technologies are also developed. Wolf et al. adapt the slot-die-coating technique to improve the cell performance by enhancing ink-substrate dynamics and surface passivation.^[62] After optimization, a high PCE of 23.8% for 2T-PSC/Si is obtained by using a textured silicon bottom cell. A blade-coating is also employed into 2T-PSC/Si for large-scale production. For example, Huang et al. develop a high-throughput blade-coating method of perovskite film on double-side-textured silicon, and a high PCE up to 26% is achieved.^[45] Those results indicate that even with cheap and simple method, the high performance could still be achieved for 2T-PSC/Si.

By constructing the 2T-PSC/Si, the V_{OC} is increased from 0.5–0.6 V of crystalline Si solar cells to 1.7–1.8 V of tandem devices. The highest V_{OC} can reach up to 1.92 V,^[50] which is about three times of single-junction Si solar cell. Albrecht et al. adopted a self-assembled, methyl-substituted carbazole monolayer to serve as the HTL in the PSC, the resulted V_{OC} and FF were reach up to 1.23 V and 84% because of the fast hole extraction and minimized nonradiative recombination at the hole-selective interface. The single PSC improvements transferred into tandem devices, which allowed a certified PCE of 29.15%. With negligible damage to efficiency, the enhanced V_{OC} can extend the application range of the device vastly, which is more beneficial for the commercial applications.

2.2. 2T Monolithic All-Perovskite Tandem Solar Cells

Due to the bandgap tune ability of perovskite solar cells,^[14a,17] all-perovskite tandem cells consisting of two perovskite absorbers with complementary bandgaps show great potential in the field of photovoltaics. The V_{OC} of 2T-PSC/PSC could be adjusted in the range of 1.66–2.30 V by matching two absorbers with different bandgaps.^[63] **Table 2** shows a summary of all the 2T-PSC/PSC.

2.2.1. CRL of 2T Monolithic All-Perovskite Tandem Solar Cells

In the 2T-PSC/PSC, the CRL plays the crucial role of efficiently recombining electrons and holes with minimal loss of voltage and reduction in transparency. Simultaneously, the deposition processes must be compatible with the underneath perovskite cells. **Table 3** summarizes the characteristics and structure of typical CRLs. Magnetron sputtering deposition of indium tin oxide (ITO) is the typical CRL, while doped organic semiconductors, ultra-thin metallic oxide, and ultra-thin metals are demonstrated better alternatives to ITO.

The first 2T-PSC/PSC was reported by Zhou et al.^[64] The novel CRL of Spiro-OMeTAD/PEDOT:PSS/PEI/PCBM:PEI (PEI = polyethyleneimine) adopts orthogonal solvent processing at low temperature, which is compatible with polar solvent-sensitive perovskite films. The CRL provides efficient space for charge recombination, 2,2',7,7'-tetrakis(*N,N*-dimethoxyphenyl-amine)9,9'-spirobifluorene (Spiro-OMeTAD) and [6,6]-phenyl-C₆₁-butyric acid methyl ester (PCBM) are employed as the hole and electron collector, respectively. While, the PEI is used to modify the surface and form a work function

Table 2. Summary of the 2T monolithic perovskite/perovskite tandem solar cells.

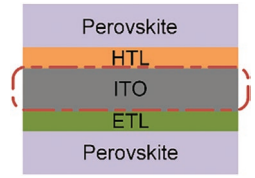
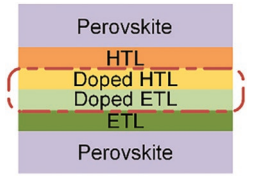
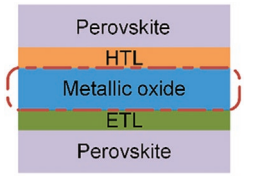
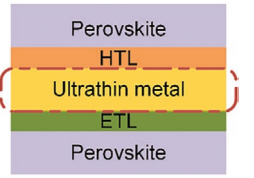
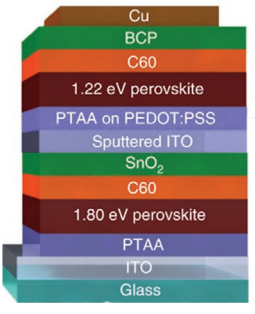
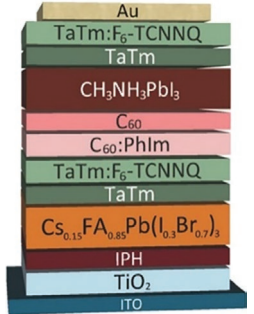
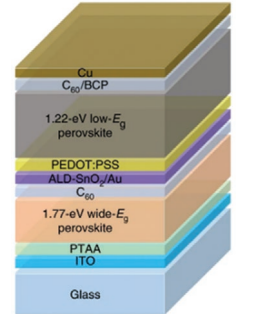
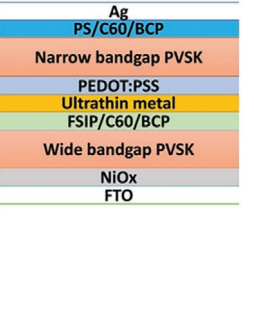
Publish date	Subcells	E_g [eV]	Absorbers	CRL	V_{OC} [V]	J_{SC} [mA cm ⁻²]	FF	PCE [%]	SOP [%]	Area [cm ²]	Ref.
2015.12	Top cell	1.55	MAPbI ₃	PEDOT:PSS	1.89	6.61	0.56	7.0	–	0.04–0.1	[64]
	Bottom cell	1.55	MAPbI ₃								
2016.11	Top cell	1.8	FA _{0.83} CS _{0.17} Pb(I _{0.5} Br _{0.5}) ₃	SnO ₂ /ZTO/ITO	1.66	14.5	0.70	16.9	17.0	0.20	[17a]
	Bottom cell	1.2	FA _{0.75} CS _{0.25} Sn _{0.5} Pb _{0.5} I ₃								
2016.12	Top cell	2	Cs _{0.15} FA _{0.85} Pb(I _{0.3} Br _{0.7}) ₃	TaTm/TaTm:F ₆ -TCNNQ/ C ₆₀ :PhIm	2.29	9.83	0.80	18.1	14.5	0.0264	[65]
	Bottom cell	1.55	MAPbI ₃								
2017.07	Top cell	1.82	MA _{0.9} CS _{0.1} Pb(I _{0.6} Br _{0.4}) ₃	ITO	1.98	12.7	0.73	18.4	18.5	0.1	[69a]
	Bottom cell	1.22	MAPb _{0.5} Sn _{0.5} I ₃								
2017.09	Top cell	2.3	MAPbBr ₃	PEDOT:PSS	1.96	6.40	0.41	5.1	–	–	[74]
	Bottom cell	1.55	MAPbI ₃								
2018.08	Top cell	1.76	FA _{0.6} CS _{0.4} Pb(I _{0.7} Br _{0.3}) ₃	SnO ₂ /ITO	1.81	14.8	0.70	–	19.1	–	[69b]
	Bottom cell	1.27	FA _{0.75} CS _{0.25} Sn _{0.5} Pb _{0.5} I ₃								
2018.09	Top cell	1.55	MAPbI ₃	TaTm/TaTm:F ₆ -TCNNQ/ C ₆₀ :PhIm	2.30	9.84	0.80	18.0	–	0.01	[63]
	Bottom cell	1.55	MAPbI ₃								
2018.10	Top cell	1.58	MAPbI ₃	p-doped cross-linked PTAA/ hexamethonium bromide- doped PC ₆₁ BM	1.79	13.36	0.78	18.7	18.92	0.12	[75]
	Bottom cell	1.26	MASn _{0.25} Pb _{0.75} I ₃								
2018.11	Top cell	1.83	FA _{0.83} CS _{0.17} Pb(Br _{0.5} I _{0.5}) ₃	ultrathin metal(s)	1.72	12.80	0.73	17.9	16.07	0.06	[71]
	Bottom cell	1.24	FA _{0.5} MA _{0.5} Pb _{0.5} Sn _{0.5} I ₃								
2018.12	Top cell	1.75	FA _{0.8} CS _{0.2} Pb(I _{0.7} Br _{0.3}) ₃	Ag/MoO _x /ITO	1.92	14.1	0.78	21	20.7	0.105	[78]
	Bottom cell	1.25	FA _{0.6} MA _{0.4} Sn _{0.6} Pb _{0.4} I ₃								
2019.02	Top cell	1.94	FA _{0.83} CS _{0.17} Pb(Br _{0.7} I _{0.3}) ₃	ITO nanoparticles	2.18	11.0	0.63	15.2	15.20	0.092	[70]
	Bottom cell	1.57	MAPbI ₃								
2019.05	Top cell	1.75	Cs _{0.05} FA _{0.8} MA _{0.15} Pb(I _{0.85} Br _{0.15}) ₃	Ag/MoO _x /ITO	1.94	15.01	0.80	23.4	23.1	0.105	[76]
	Bottom cell	1.25	FA _{0.6} MA _{0.4} Sn _{0.6} Pb _{0.4} I ₃								
2019.05	Top cell	1.7	FA _{0.6} CS _{0.3} DMA _{0.1} PbI _{2.4} Br _{0.6}	PEIE/AZO/IZO	1.88	16.0	0.77	23.1	23.0	0.08	[79]
	Bottom cell	1.27	FA _{0.75} CS _{0.25} Sn _{0.5} Pb _{0.5} I ₃								
2019.09	Top cell	1.80	FA _{0.6} CS _{0.4} Pb(I _{0.65} Br _{0.35}) ₃	SnO ₂ /ITO	1.99	15.1	0.77	23.0	22.7	0.0684	[66]
	Bottom cell	1.22	FA _{0.5} MA _{0.45} CS _{0.05} Pb _{0.5} Sn _{0.5} I ₃								
2019.09	Top cell	1.77	CS _{0.2} FA _{0.8} PbI _{1.8} Br _{1.2}	ALD-SnO ₂ /Au(=1 nm)	1.97	15.6	0.81	24.8	24.5	0.073	[67]
	Bottom cell	1.22	MA _{0.3} FA _{0.7} Pb _{0.5} Sn _{0.5} I ₃								
2020.01	Top cell	1.77	FA _{0.8} CS _{0.2} PbI _{1.8} Br _{1.2}	ALD-SnO ₂ /Au(=1 nm)	1.97	15.0	0.80	23.7	23.5	0.049	[77]
	Bottom cell	1.22	Cs _{0.1} MA _{0.2} FA _{0.7} Pb _{0.5} Sn _{0.5} I ₃								
2020.06	Top cell	1.78	CS _{0.4} FA _{0.6} PbI _{1.95} Br _{1.05}	C ₆₀ /SnO _{1.76}	2.03	15.2	0.80	24.6	24.4	0.059	[72]
	Bottom cell	1.21	Cs _{0.05} MA _{0.45} FA _{0.5} Pb _{0.5} Sn _{0.5} I ₃								
2020.08	Top cell	1.73	FA _{0.8} CS _{0.2} Pb(I _{0.7} Br _{0.3}) ₃	ITO	1.94	15.2	0.79	23.3	–	0.1	[80]
	Bottom cell	1.28	FA _{0.85} MA _{0.1} CS _{0.05} Sn _{0.5} Pb _{0.5} I ₃								
2020.09	Top cell	1.77	FA _{0.8} CS _{0.2} Pb(I _{0.6} Br _{0.4}) ₃	ALD-SnO ₂ /Au(=1 nm)	2.01	16.0	0.80	25.6	25.6	0.049	[71]
	Bottom cell	1.22	FA _{0.7} MA _{0.3} Pb _{0.5} Sn _{0.5} I ₃								

contrast between the top and bottom sides of the poly(3,4-ethylenedioxythiophene):polystyrene sulfonate (PEDOT:PSS) film. However, the noncomplementary absorption spectral region inevitably leads to low J_{SC} of 6.61 mA cm⁻² and PCE of ≈7.0%, due to the same bandgap of two absorbers. It should be mentioned that the V_{OC} of 1.89 V is almost the sum of the

two perovskite subcells, indicating a superb exploitability of 2T-PSC/PSC.

To further promote monolithic tandem cells, as mentioned afore, effective CRL is supposed to gain considerable attention. Doped organic semiconductors show a positive effect as a valuable alternative.^[65] When employing TaTm (N4,N4,N4'',N4''-

Table 3. Characteristics and structure diagrams of typical CRL.

CRL	ITO ^{a)}	Doping organic semiconductors ^{b)}	Ultra-thin metallic oxide ^{c)}	Ultra-thin metals ^{d)}
Ingredient	ITO	TaTm:F ₆ -TCNNQ/ C ₆₀ :PhIm	SnO ₂ ; AZO	Cu:Au
Preparation method	magnetron sputtering	vacuum deposition; solution spinning	atomic layer deposition	thermal evaporation
Advantages	strong protective barrier;	low-temperature; without damage; simple operation; high conductivity	low-temperature; without damage; exceptional conformality reducing shunting	low equipment demand
Disadvantages	high parasitic absorption; damage to the underlayer	no barrier protection; top subcell need vacuum deposited; low chemical stability	complicated operation; time consuming; high equipment cost	hard to be dense; complicated operation;
Structure diagram				
Device structures				

^{a)}ITO: Reproduced with permission.^[66] Copyright 2019, Springer Nature; ^{b)}Doping organic semiconductors: Reproduced with permission.^[65] Copyright 2017, Wiley; ^{c)}Ultra-thin metallic oxide: Reproduced with permission.^[67] Copyright 2019, Springer Nature; ^{d)}Ultra-thin metals: Reproduced with permission.^[68] Copyright 2018, Wiley.

tetra([1,1'-biphenyl]-4-yl)-[1,1':4',1''-terphenyl]-4,4''-diamine) and fullerene C₆₀ as HTL and ETL, respectively, F6-TCNNQ (2,2'-(perfluoronaphthalene-2,6-diylidene) dimalononitrile) and PhIm (N1,N4-bis(tri-p-tolylphosphoranylidene)benzene-1,4-diamine) are doped separately in the two layers in order to obtain function efficient CRL by modulating the conductivity. However, the CRL cannot supply protection effect, so that the top subcell needs to be deposited by vacuum method, which would make the process complicated than the simple solution. Typical MAPbI₃ subcell is applied as narrow bandgap absorber via dual source vapor deposition technique, while Cs_{0.15}FA_{0.85}Pb(I_{0.3}Br_{0.7})₃ wide bandgap absorber is combined to constitute 2T-PSC/PSC. The device shows a high efficiency of 18%, V_{OC} as high as 2.14 V, and FF of 0.76.

The application of ITO layer in 2T all-perovskite tandems was pioneered in 2016.^[17a] Employing the sputter-coated ITO to form a physical barrier to protect the underlying PSC from any solvent damage. More importantly, a buffer layer of tin oxide and ZTO, deposited before ITO via solution-deposit nanoparticles, is demonstrated to be helpful for protecting the underlying organic PCBM and perovskite layers from the sputtering of the TCO. Subsequently, introducing ITO as CRL in 2T-PSC/PSC becomes universal, and the strategy is proved to be effective.^[69] The device could reach the PCE of 23.0% with a V_{OC} of

1.99 V by sputtering ITO in a 2T-PSC/PSC as CRL. However, the high cost and inevitable damage to underneath PSC layer by high energy sputtering particles make magnetron sputtering method unsuitable for 2T-PSC/PSC. To obtain cost-effective and simple processed ITO, a solution-based method is present^[70] by spin coating ITO nanoparticles dispersed in isopropanol, which works well when combining with a PEDOT:PSS layer. To avoid solution corrosion, a further protection measure for underlying perovskite is adopted. A highly volatile acetonitrile/methylamine (ACN/MA) solution is chosen as the top absorber, and the resulting underlying perovskite is intact. Through absorber and interlayer optimization, a V_{OC} of up to 2.18 V and a steady-state PCE over 15% can be obtained, which enlightens a way of simple all solution-processed 2T-PSC/PSC.

Recently, ALD-SnO₂/Au^[67,71] and Au/Cu clusters^[68] are employed in 2T-PSC/PSC as CRL to replace the conventional ITO layer. The compact and robust ALD-SnO₂ layer is fabricated at low temperature, in order to reduce shunting with minimum damage to the bottom layer. An ultrathin Au layer (≈1 nm) is combined with ALD-SnO₂ to facilitate electron-hole recombination in the CRL, which is helpful to reach the record PCE of 25.6% of the 2T-PSC/PSC. Similarly, an ultrathin Cu:Au alloy film is also used as CRL to facilitate carrier recombination and hence achieving a high PCE up to 17.9% with a negligible

hysteresis. Besides, a simplified CRL of $C_{60}/SnO_{1.76}$ is prepared to omit the traditional HTL of top subcell because the $SnO_{1.76}$ layer has ambipolar carrier transport property. The as-prepared CRL is effective to obtain a low Ohmic contact resistance on both subcells simultaneously, leading to the PCE of 2T-PSC/PSC up to 24.4%.^[72] In future investigation of CRL, high transparency, low parasitic absorption, process-compatible, and large area fabrication process would be desired to further improve the performance of 2T-PSC/PSC.

2.2.2. Bandgap of 2T Monolithic All-Perovskite Tandem Solar Cells

Apart from effective CRL, bandgap adjustment is another key approach to improve the performance of tandem cells. Three types of 2T-PSC/PSC are divided according to different bandgaps matching, as described in Figure 6.

$MAPbI_3$ is the most classic component of perovskite solar cells. However, the absorption spectrum is merely about 400–800 nm wavelength of visible light.^[73] So it is impossible to achieve full spectrum absorption for the $MAPbI_3$ absorber, as a consequence, imperfect spectral utilization leads to the poor performance in the inchoate all-perovskite tandem structure.

Based on the well-known middle bandgap perovskite $MAPbI_3$, a better spectrum-matched middle-wide tandem solar cell can be constructed by introducing a bromated wide bandgap perovskite absorber.^[65] For the wide bandgap subcell, a perovskite with $Cs_{0.15}FA_{0.85}Pb(I_{0.3}Br_{0.7})_3$ composition is used as the absorber, which has a wide bandgap of 2 eV. The average PCE of the tandem cell is 14.8% in forward, and 15.6% in reverse bias, even not surpassing the single efficiency of $MAPbI_3$. Whereas, the V_{OC} approaches 2.3 V, which is the exact sum of the V_{OC} obtained for two subcells. Moreover, the 2T-PSC/PSC of $MAPbI_3$ matched $MAPbBr_3$ with bandgap of 2.3 eV is explored without satisfying current matching. The device shows a high V_{OC} of 1.94 V, however, the efficiency is only 5.1%.^[74] $MAPbI_3$ could also serve as middle bandgap subcell with a 1.94 eV perovskite absorber of $FA_{0.83}Cs_{0.17}Pb(Br_{0.7}I_{0.3})_3$ being used as wide bandgap subcell, as illustrated in Figure 6a–c. A solution-processed tandem architecture reaches 15.2% steady-state PCE, and delivers 2.18 V V_{OC} .^[70] The performance of middle-wide structure, as mentioned afore, is featuring high V_{OC} , whereas the efficiency is worthy of further exploration.

Middle-narrow structure in 2T-PSC/PSC is usually neglected due to the serious instability of Sn-based narrow bandgap subcells. In fact, fairly powerful improvement can be obtained for Sn-based PSCs, providing valuable opportunities for 2T-PSC/PSC contained narrow-bandgap cells. The middle-bandgap $MAPbI_3$ front subcell is connected in series with the narrow-bandgap $MASn_{0.25}Pb_{0.75}I_3$ rear subcell by a solution-processed conductive CRL, as shown in Figure 6d–f.^[75] Importantly, long-term stable tandem cells are also demonstrated by employing ALD Al_2O_3 film as the encapsulation layer, maintaining ~91% of its initial efficiency after more than 9300 h (~387 days) of air storage, and the devices exhibit encouragingly a remarkable PCE up to 18.69% with a V_{OC} of 1.79 V.

The current matching is crucial for the improvement of 2T tandem solar cells, which can be adjusted by manipulating the

thickness and the bandgap of the two absorbers. The optimized devices would match a narrow-bandgap of 0.9–1.2 eV for top subcell and a wide-bandgap of 1.7–1.9 eV for bottom subcell.^[14a] A perovskite solar cell with stable 14.8% PCE is demonstrated, based on an ~1.2 eV $FA_{0.75}Cs_{0.25}Pb_{0.5}Sn_{0.5}I_3$ absorber by a precursor-phase antisolvent immersion technique. While combining the narrow bandgap absorber with a 1.8 eV $FA_{0.83}Cs_{0.17}Pb(I_{0.5}Br_{0.5})_3$ perovskite cell, the tandem device achieves efficiency of 17.0% with a V_{OC} over 1.65 V, as shown in Figure 6g–i.^[17a]

In recent years, the tandem devices are further developed with the enhancement on the performance of narrow bandgap PSCs. Optimizing the narrow-bandgap perovskite nearly becomes the universal path of all-perovskite tandem devices. A small bandgap perovskite $MAPb_{0.5}Sn_{0.5}I_3$ of 1.22 eV is improved by employing Indene- C_{60} bis-adduct to achieve optimized interfacial contact and reduced nonradiative recombination.^[69a] The resultant 2T-PSC/PSC, combined with large bandgap absorber of $MA_{0.9}Cs_{0.1}Pb(I_{0.6}Br_{0.4})_3$ and CRL of sputtered ITO, shows a high V_{OC} of 1.98 V and stabilized PCE of 18.5%. A method to post-process the $FA_{0.75}Cs_{0.25}Sn_{0.5}Pb_{0.5}I_3$ perovskite films with methylammonium chloride vapor is adopted to enhance the narrow-bandgap perovskite.^[69b] By optimization of grain sizes and film flatness, the efficiency could be raised to 15.6% with an external quantum efficiency (EQE) of over 80% in the near-infrared with superior thermal, atmospheric, and operational stability. Then, a 50 nm highly conductive ITO interlayer is supplied as a CRL to protect the wide-bandgap perovskite before depositing $FA_{0.75}Cs_{0.25}Sn_{0.5}Pb_{0.5}I_3$ as the top subcell. As a result, the 2T-PSC/PSC shows a high V_{OC} of 1.98 V and PCE of 19.1%.

Furthermore, with the optimization of narrow bandgap cells, the prominent improvement on both the PCE and stability of Sn-Pb perovskites has been obtained.^[76] The solution of reducing the grain defect density is certified by modifying GuaSCN and adding metallic tin powders in precursor. By increasing the charge-carrier diffusion length in Sn-Pb perovskites to 3 μm , the improved narrow bandgap cell can achieve PCE of 21.1%. A 1.75 eV PSC is adopted as wide-bandgap absorber to design tandem device. The resultant stable power output efficiency is ~23.1%, and the obtained V_{OC} is up to 1.94 V.

The superb narrow-bandgap solar cell of 1.22 eV with PCE of 21.2% is combined with complementary 1.77 eV wide-bandgap top subcell, and the device exhibits the PCE of 24.8% with a high V_{OC} of 1.97 V. In theoretical perspective, PCE over 39% is achievable using an optimal bandgap combination of 1.1–1.15 eV and 1.75 eV in a 2T configuration. Moreover, PEA^+ additive is used in the antisolvent to anchor the Sn-Pb perovskite grains without excess formation of layered perovskite phases. The suppressed nonradiative carrier recombination in Sn-Pb perovskite active layers boosts the whole 2T-PSC/PSC device a stabilized PCE of 23.5%.^[77]

PSCs can work with thickness of merely a few hundred nanometers, moreover, the solution-processable property of PSCs enables large-area printing and flexibility, which can significantly reduce the cost and extend the applications. Combining the PSCs to construct 2T-PSC/PSC can extend the V_{OC} and flexibility effectively. Therefore, further advances in 2T perovskite tandem devices become an exciting scientific challenge and hold enormous potential.

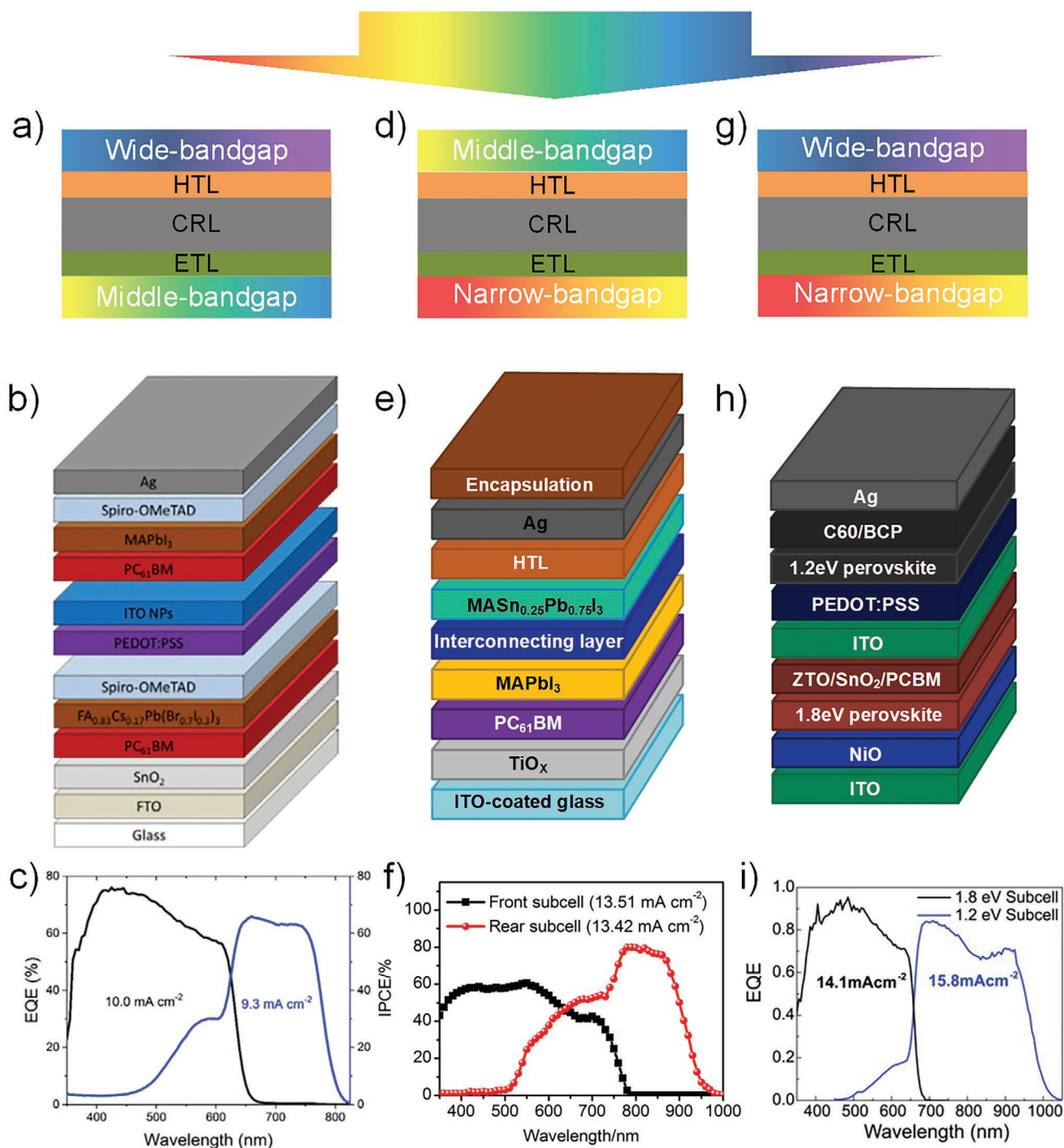


Figure 6. The structure diagrams and EQEs curves of 2T-PSC/PSC combined with different matched bandgaps. a–c) A tandem device with middle and wide bandgaps. Reproduced with permission.^[70] Copyright 2019, Elsevier B.V. d–f) A tandem device with middle and narrow bandgaps. Reproduced with permission.^[75] Copyright 2018, Elsevier B.V. g–i) A tandem device with wide and narrow bandgaps. Reproduced with permission.^[17a] Copyright 2016, American Association for the Advancement of Science.

2.3. 2T Monolithic Perovskite/Organic Tandem Solar Cells

Organic solar cell is a striking sort of solar cells, which benefits mainly from its high transmittance, flexibility, and solvent processing.^[81] Although the single-junction organic photovoltaic

(OPV) with over 17% PCE is demonstrated,^[13] the V_{OC} of majority devices can merely reveal around 0.8 V.^[82] In order to improve the V_{OC} , combining with another absorber to extend the spectral absorption region is a viable approach. OPV has numerous characteristics, which are suitable for fabricating

Table 4. Summary of the 2T monolithic perovskite/organic tandem solar cell.

Publish date	Perovskite absorber	E_g [eV]	Organic absorber	CRL	V_{OC} [V]	J_{SC} [mA cm^{-2}]	FF	PCE [%]	Ref.
2015.01	MAPbI ₃	1.52	PBSeDTEG8:PCBM	FEN/TiO ₂ /PEDOT:PSS	1.52	10.05	0.67	10.23	[84]
2016.01	MAPbI ₃	1.5	PBDTT-DPP:PC70BM	PFN/Ag-doped MoO ₃ /MoO ₃	1.58	8.02	0.68	8.62	[87]
2016.02	MAPbI ₃	1.5	PCE-10:PC71BM	C ₆₀ -SB/Ag/MoO ₃	1.63	13.1	0.75	16.0	[85]
2019.05	CsPbI ₂ Br	1.92	PTB7-Th:CO ₂ DFIC:PC ₇₁ BM	MoO ₃ /Au/ZnO	1.71	11.98	0.73	15.04	[88]
2020.03	Cs _{0.1} (FA _{0.6} MA _{0.4}) _{0.9} Pb(I _{0.6} Br _{0.4}) ₃	1.74	PBDB-T:SN6IC-4F	Ag	1.85	11.52	0.71	15.13	[86]
2020.06	FA _{0.8} MA _{0.02} Cs _{0.18} PbI _{1.8} Br _{1.2}	1.77	PBDBT-2F:Y6:PC71BM	Ag	1.90	13.05	0.83	20.6	[89]
2020.07	CsPbI ₂ Br	1.9	PM6:Y6	MoO ₃ /Ag/ZnO	1.95	12.46	0.76	18.38	[90]

2T-PSC/OPV, such as higher absorption in the near-infrared region and the low-cost solution process. Adjusting the intramolecular electron push-pulling effects makes the energy levels and absorbance range highly tunable.^[83] All the 2T-PSC/OPV are summarized as **Table 4**.

In 2015, Yang group^[84] demonstrated a structure of 2T-PSC/OPV. 1.55 eV MAPbI₃ is employed as bottom subcell, and an IR-sensitive block copolymer (PBSeDTEG8) is used as the top absorber. The CRL is constituted of PFN/TiO₂/PEDOT:PSS PH500/PEDOT:PSS AI 4083, which is the ETL from the top cell and HTL from the bottom cell, as demonstrated in **Figure 7a–c**. The whole tandem device is prepared through solution method, which takes full advantage of the organic solar cell. The absorption spectrum is expanded up to 950 nm and the V_{OC} is enhanced to 1.52 V. However, the PCE is limited to 10.23%, only slightly higher than the single subcells.

To prevent the organic layer from the damage of high temperature and solvent erosion when deposit perovskite layer, the preparing sequence of each layer is adjusted.^[85] The organic layer is employed as bottom subcell for the tandem structure, as depicted in **Figure 7d–e**. Combining the MAPbI₃ perovskite top subcell and PCE-10:PC71BM polymer:fullerene blended bottom subcell, a high PCE up to 16.0% is achieved. The upgrading of the photovoltaic performance is also credited to the graded CRL containing a zwitterionic fullerene, silver (Ag), and molybdenum trioxide (MoO₃), which provide robust protection for front subcell. Nevertheless, the EQE profiles of the perovskite and polymer single-junction solar cells show the overlapping spectrum in IR range, resulting in the V_{OC} of only 1.65 V.

Recently, a bandgap well-matched 2T-PSC/OPV is developed to satisfy the requirements of spectrum expansion and minimize parasitic absorption.^[86] The phenmethylammonium bromide passivated Cs_{0.1}(FA_{0.6}MA_{0.4})_{0.9}Pb(I_{0.6}Br_{0.4})₃ is served as top subcell (1.74 eV), and organic active PBDB-T:SN6IC-4F layer is used as bottom subcell (1.30 eV). Appropriate bandgap matching of the monolithic device broadened the absorption spectrum from 300 to 975 nm, resulting in a high V_{OC} up to 1.85 V, and the PCE is still maintained above 15%.

The substantive breakthrough of 2T-PSC/OPV is demonstrated under the calculated instructing.^[89] 1.77 eV wide band-gap FA_{0.8}MA_{0.02}Cs_{0.18}PbI_{1.8}Br_{1.2} perovskite and 1.41 eV OPV are selected as two subcells (**Figure 7g–i**). As shown in EQE curves, the J_{SC} of front and rear subcells is exactly the same, 13.1 mA cm⁻², indicating the good spectra matching. Benefiting from orthogonal processing solvents, the CRL

could be simplified by all-thermal evaporation including BCP, Ag, and MoO_x, which possesses negligible optical loss and high reproducibility. The PCE of the tandem device is 20.6%, which is higher than that of each separate subcell. The integrated V_{OC} is approximately close to the summing voltage of two subcells. The landmark performance of 2T-PSC/OPV is established, on the basis of which we can look forward to the further improvement.

The organic absorber and perovskite absorber are solution-processed, which lay the foundation of fabricating flexible devices. Similar to the 2T-PSC/PSC, 2T-OPV/PSC has potential for high throughput manufacture of flexible electronic devices. Besides, benefiting from the orthogonal processing solvents, the requirements for CRLs are more lenient and the preparation of 2T-OPV/PSC is terser correspondingly.

2.4. 2T Monolithic Perovskite/CIGS Tandem Solar Cell

Cu(In,Ga)(S,Se)₂ (CIGS) and CuIn(S,Se)₂ (CIS) are also alternative bottom cell candidates with low bandgap for perovskite-based tandem solar cells, revealing unique merits. The direct bandgap structure implies the superior photovoltaic properties, as confirmed by the realistic efficiency of 23.4%.^[13]

In terms of bandgap, CIGS can be tuned from 0.95 to 1.7 eV by substituting Ga and S for In and Se, respectively,^[91] which is predicted to afford excellent current matching in monolithic tandem devices with the high efficiency PSCs. Moreover, CIGS absorbers have solution-processable and cost-effective advantages, promising 2T-PSC/CIGS to become competitive applications in photovoltaic field as certified in **Table 5**.

The initial 2T-PSC/CIGS consisted of a 1.04 eV CIGS solar cell and a 1.72 eV PSC was demonstrated by Todorov et al., enabling PCE of 10.98% and V_{OC} up to 1.45 V,^[92] as shown in **Figure 8a–c**. The perovskite layer is prepared by vapor-based halide exchange reaction system to control annealing temperature below 150 °C, resulting in better compatibility with the CIGS subcell. However, the perovskite with ZnO acts as ETL is tend to degrade by the surface active hydroxyl, when exposing to UV excitation and high temperature of above 60 °C, which could be avoided to a certain extent by the surface coating. Therefore, the classical ZnO layer in CIGS device is removed to prevent perovskite deterioration, sacrificing the performance of the CIGS to a certain extent. Furthermore, the limited J_{SC} is attributed to the Ca-based contact electrode, which absorbs

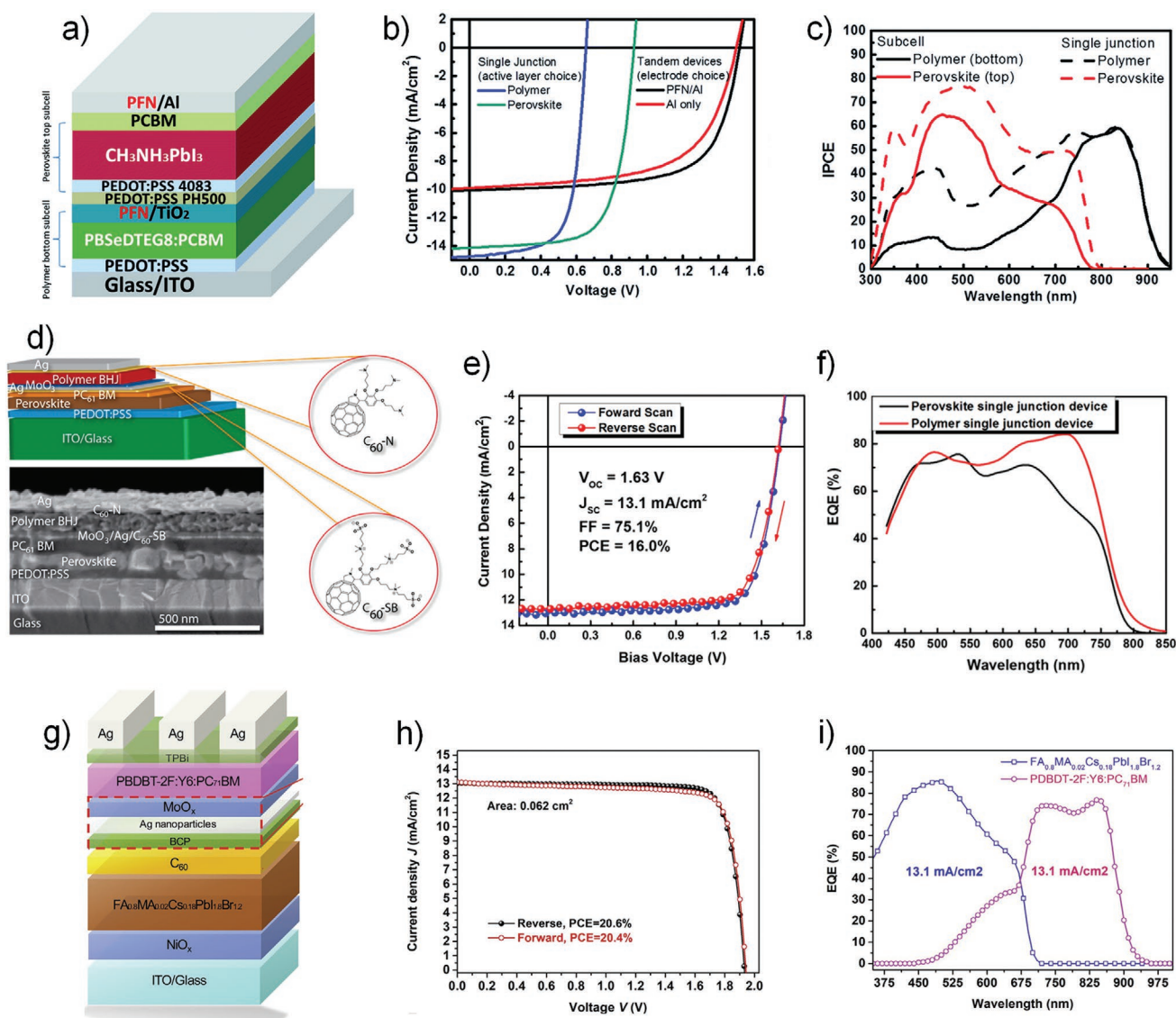


Figure 7. a–c) The first 2T-PSC/OPV. a) Device architecture; b) J – V curves; c) EQE spectra. Reproduced with permission.^[84] Copyright 2015, The Royal Society of Chemistry. d–f) The order of deposition is adjusted perovskite/polymer monolithic tandem solar cell. d) Device architecture; e) J – V curves and device metrics; f) EQE spectra. Reproduced with permission.^[85] Copyright 2016, American Chemical Society; g–i) The bandgaps optimized perovskite/organic monolithic tandem solar cell. g) Device architecture; h) J – V curves; i) EQE spectra. Reproduced with permission.^[86] Copyright 2019, Science China Press.

about 20–30% of incident light. However, due to serious parasitic optical losses, the J_{SC} is severely limited to 12.7 mA cm^{-2} , and the PCE is much lower than the individual subcells.

Subsequently, a multilayer transparent top electrode is developed. The delicate dielectric/metal/dielectric ($\text{MoO}_x/\text{Ag}/\text{MoO}_x$) structure is employed to 4T-PSC/CIGS, enabling a PCE of 15.5%.^[89] Noteworthy, it supplied a promising route to further optimize 2T-PSC/CIGS. On the basis of Yang's work, the tandem device can realize transparent top electrode, such as the aluminum-doped zinc oxide (AZO) layer, rendering about 40% of the red light (650–750 nm) is transmitted.

As mentioned previously, how to reserve the ZnO layer is a barrier on the high-performance pursuit. Whereafter, a ZnO-contained 2T-PSC/CIGS was developed in the early period.^[93]

The deposited intrinsic ZnO layer could guarantee the integrality before the AZO layer, resulting in a preferable PCE of 11.03% and a V_{OC} of 1.35 V. The necessity to maintain the integrality of the CIGS subcell has been verified repeatedly.^[94] An i-ZnO and boron-doped ZnO double layer is developed as the TCO layers of the bottom cell and a smooth ITO is used as the CRL. The maximum vertical distance of ITO-polished surface is reduced from several hundred nm to 40 nm, which is beneficial for the continuous deposition of the planar perovskite subcell and takes full advantages of the top subcell. The resultant tandem device delivers the PCE of 22.43% and the V_{OC} of 1.774 V, equal to the sum of the V_{OC} of two subcells.

Another effective approach to prevent potential shunting due to the rough CIGS surface was reported by conformally

Table 5. Summary of the 2T monolithic perovskite/CIGS tandem solar cell.

Publish month	Subcells	Absorbers	E_g [eV]	CRL	V_{oc} [V]	J_{sc} [mA cm^{-2}]	FF	PCE [%]	Area [cm^2]	Ref.
2015.09	Top subcell	$\text{MAPb}(\text{Br}_{1-x}\text{I}_x)_3$	1.72	ITO	1.45	12.7	0.57	10.9	0.4	[92]
	Bottom subcell	CIGS	1.04							
2017.01	Top subcell	MAPbI_3	1.59	ZnO/ITO	1.36	15.5	0.88	18.5	0.11	[96]
	Bottom subcell	CIS	0.99							
2017.08	Top subcell	MAPbI_3	1.59	iZnO/AZO	1.35	12.9	0.64	11.03	0.5	[93]
	Bottom subcell	CIS	1.0							
2018.08	Top subcell	MAPbI_3	1.6	ZnO/ITO	1.38	13.8	0.44	8.34	0.11	[97]
	Bottom subcell	CIS	1.0							
2018.08	Top subcell	$\text{Cs}_{0.09}\text{FA}_{0.77}\text{MA}_{0.14}\text{Pb}(\text{I}_{0.86}\text{Br}_{0.14})_3$	1.59	iZnO/BZO/ITO	1.77	17.3	0.73	22.43	0.042	[94]
	Bottom subcell	CIGS	1.0		1.78	16.67	0.70	20.83	0.52	
2019.01	Top subcell	$\text{Cs}_{0.05}(\text{MA}_{0.17}\text{FA}_{0.83})_{0.95}\text{Pb}_{1.1}(\text{I}_{0.83}\text{Br}_{0.17})_3$	–	ZnO/NiO _x	1.59	18.0	0.76	21.6	0.778	[95]
	Bottom subcell	CIGS	1.1							

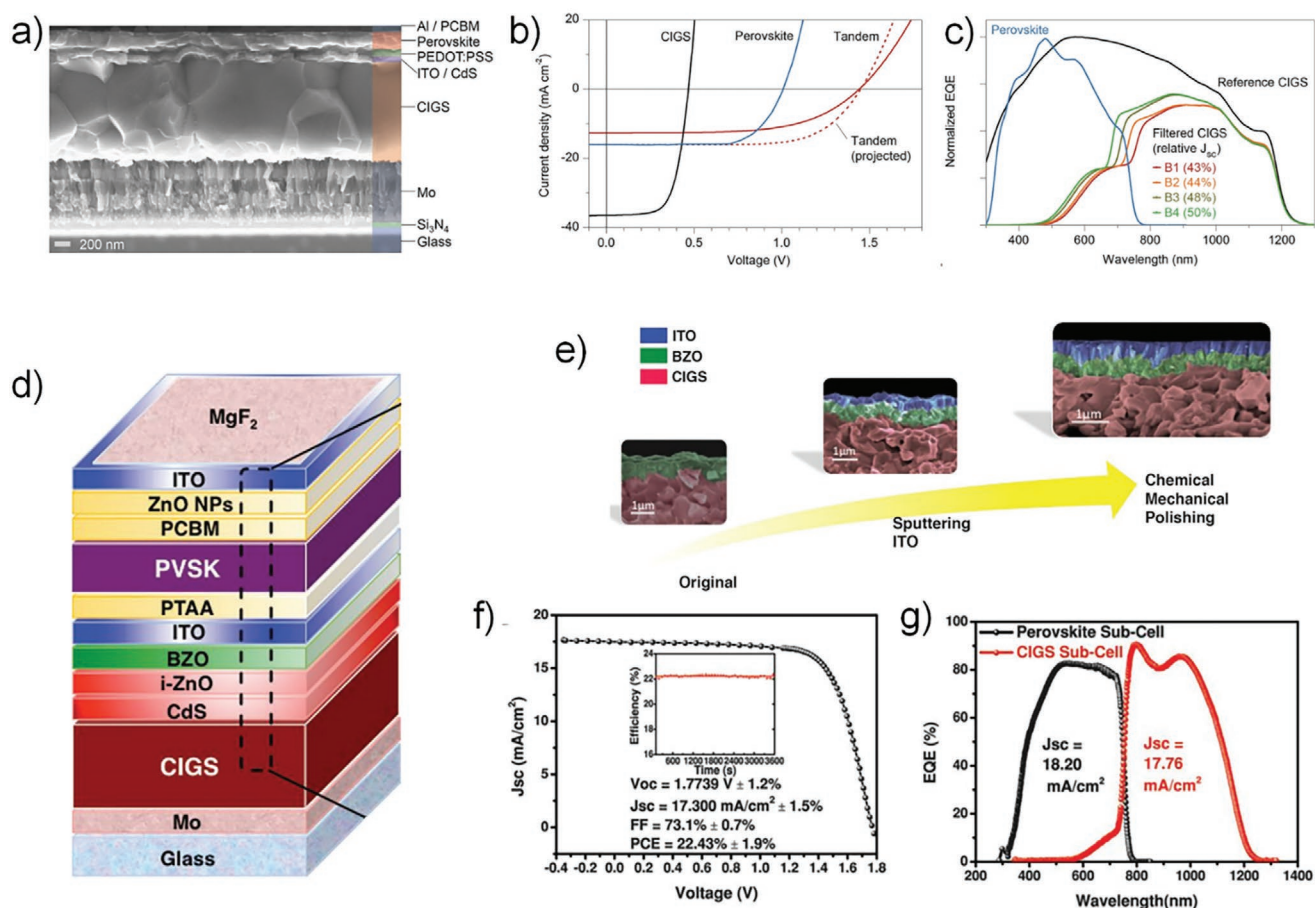


Figure 8. a–c) The first 2T-perovskite/CIGS without ZnO layer. Reproduced with permission.^[92] Copyright 2018, Wiley. d–g) The optimized 2T-perovskite/CIGS reserved ZnO layer. d) Schematic; e) cross-sectional SEM images of the CMP processing on the CIGS surface; f) J - V curves; g) EQE curves. Reproduced with permission.^[94] Copyright 2015, American Association for the Advancement of Science.

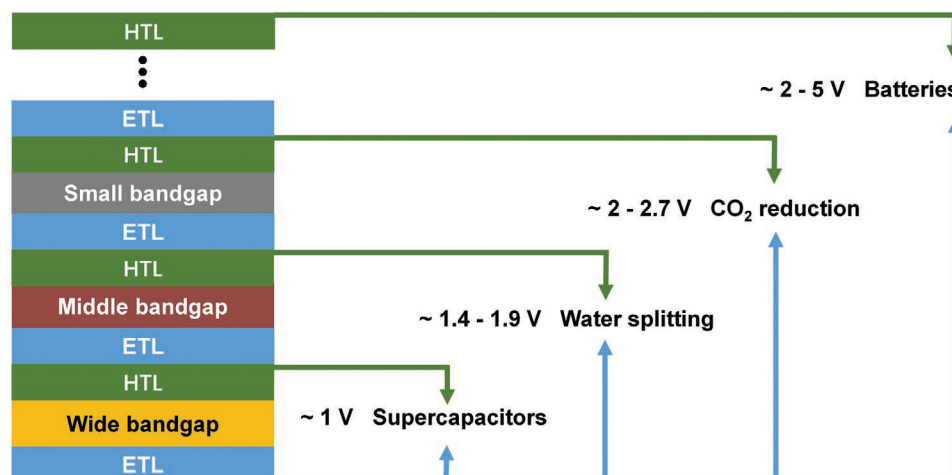


Figure 9. The tandem cells with adjustable V_{OC} to drive different solar energy conversion and storage.

depositing a thin NiO_x layer on the front contact of the CIGS bottom cell.^[95] After constructing a bilayer of the NiO_x /PTAA, the 2T-PSC/CIGS shows a high V_{OC} of 1.59 V, and the PCE of 21.6% on the large active area of 0.778 cm², which is the highest PCE reported for a perovskite/CIGS tandem solar cell with the conventional area of 0.2 cm².

CIGS solar cells are promising candidate to replace the Si solar cells in commercial application. Correspondingly, the 2T-PSC/CIGS shows high V_{OC} and steady growing PCE. However, more efforts need to be made to overcome the potential efficiency loss, such as the matched bandgap, performance of subcells, well-designed CRL, or other aspects. With those improvements, it is likely to enable the predicted efficiencies of over 30% in the near future.

3. Potential Application for Energy Conversion and Storage

The solar cells can drive the energy conversion from solar energy to electric energy, however, the obtained electric energy is limited by the instability and intermittent of solar irradiation. As for single-junction solar cells, the low output voltage is also a huge obstacle for potential applications of clean energy. This unstable source of power is hardly to be linked up directly for practical equipments. Thus, storing the solar energy as chemical energy becomes an effective way to harness solar energy. Nowadays, some solar energy conversion and storage systems have attracted intense interest, such as low-voltage solar rechargeable supercapacitors, middle-voltage solar-driven water-splitting and CO₂ reduction, as well as high-voltage solar rechargeable batteries. Since PSCs have the tunable bandgap and high V_{oc} among various types of solar cells, more attentions are suggested to PSC-based tandem cells with high voltage and efficiency in future. When introducing tandem solar cells to provide higher voltage, which could break the Shockle–Queisser (S-Q) limitation, the derived solar energy conversion and storage hybrid systems become extremely inviting as shown in **Figure 9**. In order to achieve the energy conversion/storage, the voltage matching principle is pivotal

for constructing those integrated devices. It means that the V_{oc} in PSC-based tandem cells must surpass the electrochemical working window to ensure a feasible energy conversion/storage. Meanwhile, the maximum power point should be as close to the charge/reaction voltage plateau for high overall efficiency. In this way, rechargeable reactions with specific voltage plateau are more favorable in those integrated energy conversion/storage devices.

3.1. Solar Rechargeable Supercapacitors

In terms of supercapacitors, the voltage demands could be relatively low, making it possible for a simple solar rechargeable supercapacitors structure to realize the photoelectric energy conversion and electrochemical energy storage. Reserving the solar energy as chemical energy can avoid the instability from light intensity fluctuations or the diurnal cycle. Benefiting from intrinsic excellent electrical feature, solar rechargeable supercapacitors could provide continuous output of electric power with tunable high power density.^[98]

Due to the low cost and the high efficiency, PSCs become the most potential power supply source. In a traditional design, PSCs and supercapacitors are connected by external circuits to realize the integration of photoelectric conversion and electrical energy storage.^[99] The first configuration of solar-driven supercapacitors, based on a state-of-the-art MAPbI₃ solar cell, was demonstrated by Wang et al. (**Figure 10a,b**).^[99a] They combined an energy pack containing MAPbI₃ solar cell and polypyrrole-based supercapacitor in series, providing the overall conversion efficiency of 10% and output voltage of 1.45 V from both the supercapacitor and PSC. A supercapacitor with improved performance was also prepared.^[99b] The self-stacked solvated graphene film as independent electrode is used to fabricate a flexible solid supercapacitor, exhibiting a high specific capacitance of 245 F g⁻¹ at 1 A g⁻¹ and retaining 83% of its original values after 10 000 cycles. Three supercapacitors are further connected with state-of-the-art perovskites through two-copper wires, realizing the integration of photoelectric conversion and electrical energy storage.

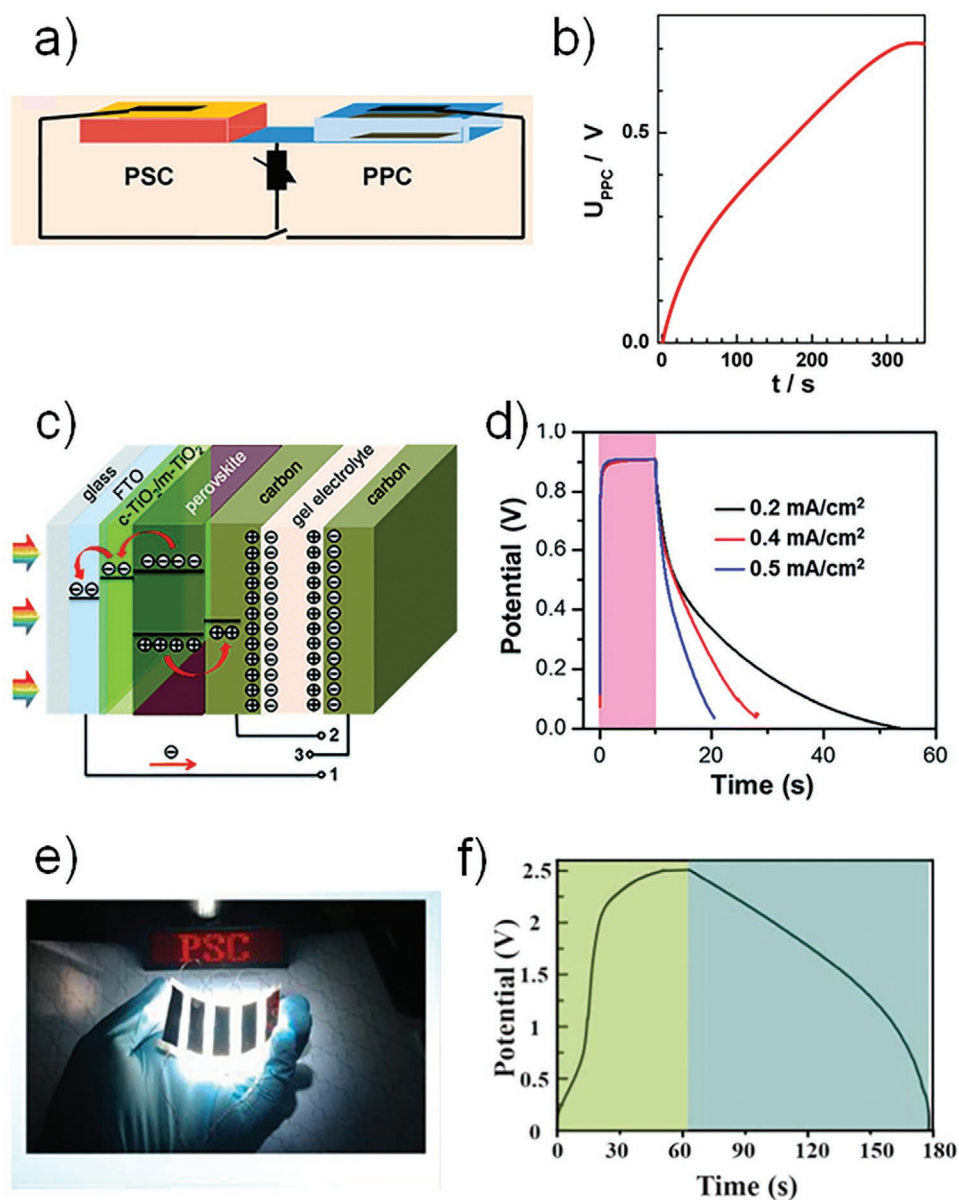


Figure 10. a,b) Integrated energy pack connected by wires containing a MAPbI₃-based solar cell and a polypyrrole-based supercapacitor. Reproduced with permission.^[99a] Copyright 2015, American Chemical Society. c,d) Integrated photo-supercapacitor used a nanocarbon co-anode. Reproduced with permission.^[104a] Copyright 2018, The Royal Society of Chemistry. e,f) "Bamboo slip" architecture gathered five photocapacitors. Reproduced with permission.^[106] Copyright 2018, Elsevier B.V.

The wire-connected separated pattern is quickly replaced by sharing an electrode, as its low integration and waste of cost and space are not compatible with future application. PEDOT-carbon electrode was employed to bridge photoelectric conversion unit and energy storage part by playing double functions of both holes collector from perovskite and electrode materials for redox supercapacitors.^[100] The realized integrated photo-supercapacitor delivers a maximum efficiency up to 4.70% with a high energy storage efficiency of 73.77%. Co-anode photo-supercapacitors also were frequently reported, including Janus carbon paper,^[98] Au,^[101] silver epoxy,^[102] carbon nanotube,^[103] nanoporous carbons (Figure 10c,d).^[104] Furthermore, there still

co-cathode system was applied, such as the fluorine-doped tin oxide served as the cathode for both PSCs and electrochromic supercapacitors.^[101]

The design and fabrication of photo-supercapacitor by integrating a PSC unit and a supercapacitor unit into a single device without wires are aiming to avoid unnecessary external connections and promote the level of integration. However, with the increasing demands of high operating voltage, high output voltage of photo-supercapacitor becomes an important parameter to pursue. Four individual photo-supercapacitors are assembled together in series with an active area of 7.5 cm² and delivered ≈3.8 V stable output voltage, which successfully drive

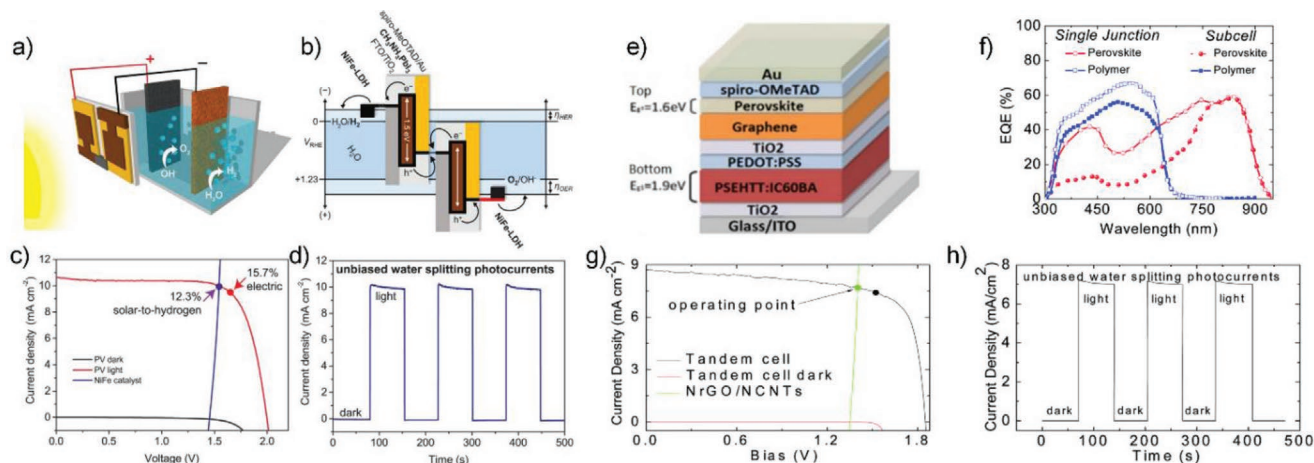


Figure 11. a–d) Combination of the series perovskite cells with NiFe DLH/Ni foam electrodes for water splitting. a) Schematic diagram of the water-splitting device. b) A generalized energy schematic of the series perovskite cells for water splitting. c) J - V curves of the series perovskite cell and the NiFe/Ni foam electrodes in a two-electrode configuration. d) Current density–time curve of the integrated water splitting device without external bias. Reproduced with permission.^[108] Copyright 2014, American Association for the Advancement of Science. e–h) Configuration of perovskite/organic tandem solar cells with NRG/NCNT electrocatalyst for water splitting. Reproduced with permission.^[107] Copyright 2016, The Royal Society of Chemistry.

light-emitting diodes (LEDs) after being photo-charged.^[105] Every monomer is made of carbon-counter electrode-based PSC and MnO_2 asymmetric solid-state supercapacitor. A MAPbI_3 PSC and supercapacitor are integrated with hybrid electrode of $\text{CC-Co}_3\text{S}_8\text{-MnO}_2$ on bi-polar TiO_2 nanotube arrays and woven five photo-capacitors into “bamboo slip” architecture by silk used as the “hide ropes,” as shown in Figure 10e,f.^[106] The system ultimately achieved output voltage over 2.4 V, which is enough to power the LED light and electric fan.

The solar rechargeable supercapacitors have great advantages in promoting utilization of green energy and facilitating the portable power supply technologies. From the developed perspective of solar rechargeable supercapacitors, higher voltage could help improving energy density, thus efficient high voltage 2T-PBTSCs have the potential for achieving better integrated devices.

3.2. Hydrogen Production by Solar Water-Splitting

Highly effective production and utilization of hydrogen based on the water circle is the “Holy-Grail” of clean energy. In recent years, solar water-splitting system has attracted a great attention, however, it still remains a great challenge to develop low-cost and high efficiency devices. Theoretically, water-splitting requires a thermodynamic driving force about 1.23 V, considering the unavoidable polarization, the practically operating voltage is varied from 1.4 to 1.9 V.^[107] Single-junction solar cells cannot provide such relatively high voltage, while tandem devices could satisfy these demands.

Therefore, introducing serial connected solar cells with a high voltage is a reasonable method to drive electrolysis of water. Grätzel group^[108] first made an attempt to design an efficient water-splitting device by connecting two PSCs in series. The solar cell module on the basis of state-of-the-art MAPbI_3 absorber presents V_{OC} of 2.00 V and PCE of 15.7%. The predicted operating current density of the combined

system gives a value of 10.0 mA cm^{-2} , corresponding to a solar-to-hydrogen efficiency of 12.3%, as shown in Figure 11a–d. Two perovskite cells connecting in series could offer nearly 2.00 V to drive water-splitting, showing great advantage over the low-voltage cells, such as three-series silicon,^[109] and III–V-based solar cells.^[110] It is a great progress on the way to form an integrated device system.

Hybrid perovskite tandem solar cells can push further device integration, as demonstrated in Figure 11e–h.^[107] The 2T monolithic tandem architecture is constructed by a solution-processed wide bandgap polymer top subcell and a perovskite MAPbI_3 bottom cell, exhibiting V_{OC} of 1.86 V and PCE of 11.28%. Effective nonprecious electrocatalyst for hydrogen evolution and oxygen evolution in an alkaline medium is combined with the tandem solar cells to fabricate the integrated water-splitting device, showing a high overall efficiency of 9.02% for solar-to-hydrogen conversion.

Based on the previous investigations, the device integration from multiple single-junction cells to monolithic tandem cells is feasible. The tandem solar cells can provide high enough output voltage with improved PCE. Especially, the 2T PSC-based tandem solar cells could satisfy the voltage requirement for water-splitting directly, as well as achieving photo-electrochemical conversion in an integration device.

3.3. Solar-Driven Conversion of Carbon Dioxide

CO_2 reduction is an efficient approach to acquire useful chemicals and fuels mainly as CO and hydrocarbon oxygen, which also makes great contribution to decreasing the concentration of CO_2 in the atmosphere simultaneously. When driving by solar energy, this conversion process would be extremely attractive as an artificial photosynthesis conception. Since the driving voltage demand is too high to be afforded by merely single-junction solar cells, resorting to tandem solar cells would be a rational choice.

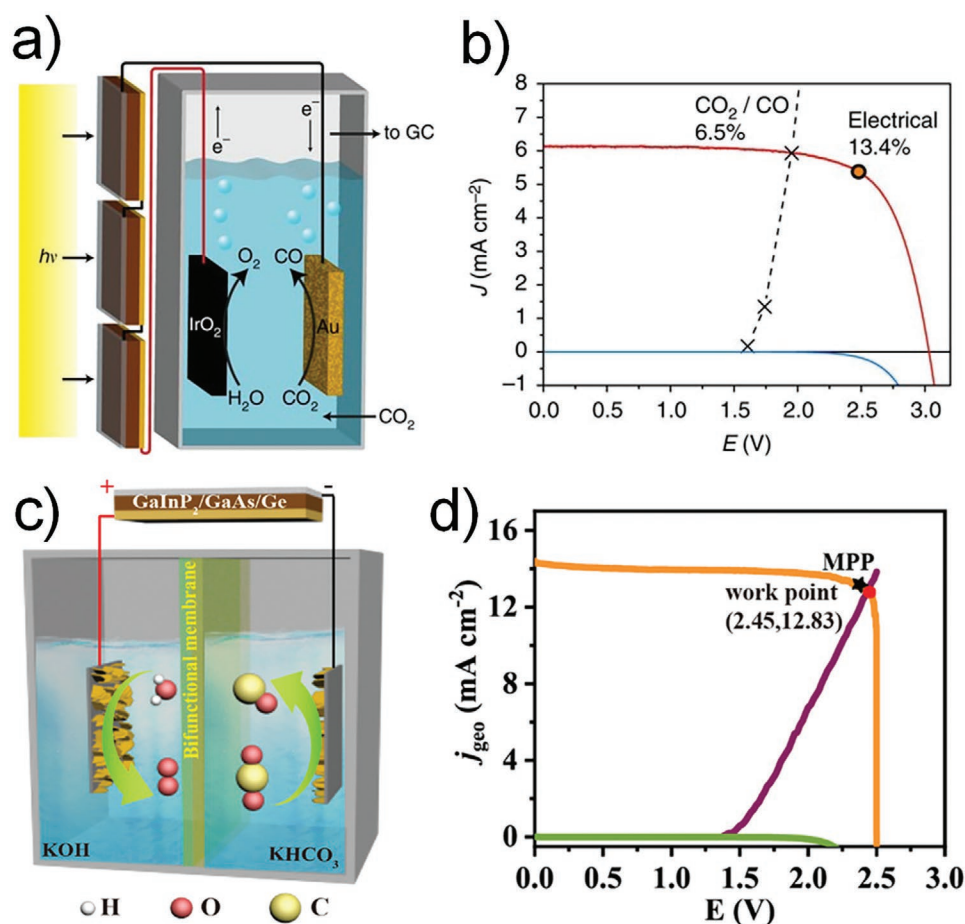


Figure 12. a,b) Series-connected three perovskite cells-driven CO₂ reduction system. a) Schematic diagram; b) *J*–*V* curves of three series-connected perovskite cells under simulated AM 1.5G 1 Sun solar irradiation and in the dark, overlaid with the matched *J*–*V* characteristic of the CO₂-reduction and oxygen-evolution electrodes. Reproduced with permission.^[112] Copyright 2015, Springer Nature. c,d) GaInP₂/GaAs/Ge tandem solar cells-driven CO₂ reduction system. c) Schematic diagram; d) *J*–*V* curves of the GaInP₂/GaAs/Ge tandem solar cell under simulated AM 1.5 G 1 Sun solar irradiation. Reproduced with permission.^[113] Copyright 2020, Wiley.

The reduction chemicals have kinds of types, such as CO, HCOOH, CH₃OH, CH₄, C₂H₄, C₂H₅OH, CH₃COOH, C₃H₈O. In the CO₂-to-CO conversion process, apart from the thermodynamic potential 1.34 V for the cathode reduction and water oxidation at the anode, extra overpotential for C₂₊ product formation and water oxidation are acquired. Consequently, the device must provide a resulting voltage of at least 2 V or more to driven the system work.^[111] Single-junction solar cells hardly afford the high working voltage, so the series-connected solar cells used for CO₂ reduction system arise at the historic moment. PSCs were applied to the CO₂ conversion in a series of three junctions initially with *V*_{OC} of 3.1 V, and finally a solar-to-CO efficiency about 6.5%,^[112] shown as **Figure 12a,b**. However, the series solar cells have decreased treble the *J*_{SC} and PCE because of the increased irradiation area.

There could be a better choice to supply the voltage by introducing a tandem solar cell, which can markedly simplify the device structure and decrease the fabrication cost. The three-junction GaInP₂/GaAs/Ge solar cells are commonly used for driving elements, accompanying by a sufficient *V*_{OC} of 2.5 V and a high *J*_{SC} greater than 14 mA cm⁻².^[113] In the

tandem solar cell-driven system, the operating current was observed to be 13.1 mA cm⁻² from the intersection point, hence the solar-to-CO efficiency reached 15.5%, very close to the maximum power point for the solar-to-electric energy conversion, shown as **Figure 12c,d**. Recently, Tan et al. report an all-perovskite triple-junction solar cells with PCEs over 20% and *V*_{OC} up to 2.80 V.^[114] Simultaneously, Janssen and co-workers present a triple-junction perovskite tandem, showing very promising PCE of 16.8%, with a *V*_{OC} of 2.78 V.^[115] Given the rapid progress in triple-junction perovskite tandem cells, it is anticipated that the perovskite-driven conversion of carbon dioxide with high efficiency and low cost could be achieved in the near future.

3.4. Solar Rechargeable Batteries

High energy rechargeable batteries are common and important energy storage devices in our society. The infinite solar energy could be converted to chemical energy, which would be directly stored into battery systems for subsequent utilization.

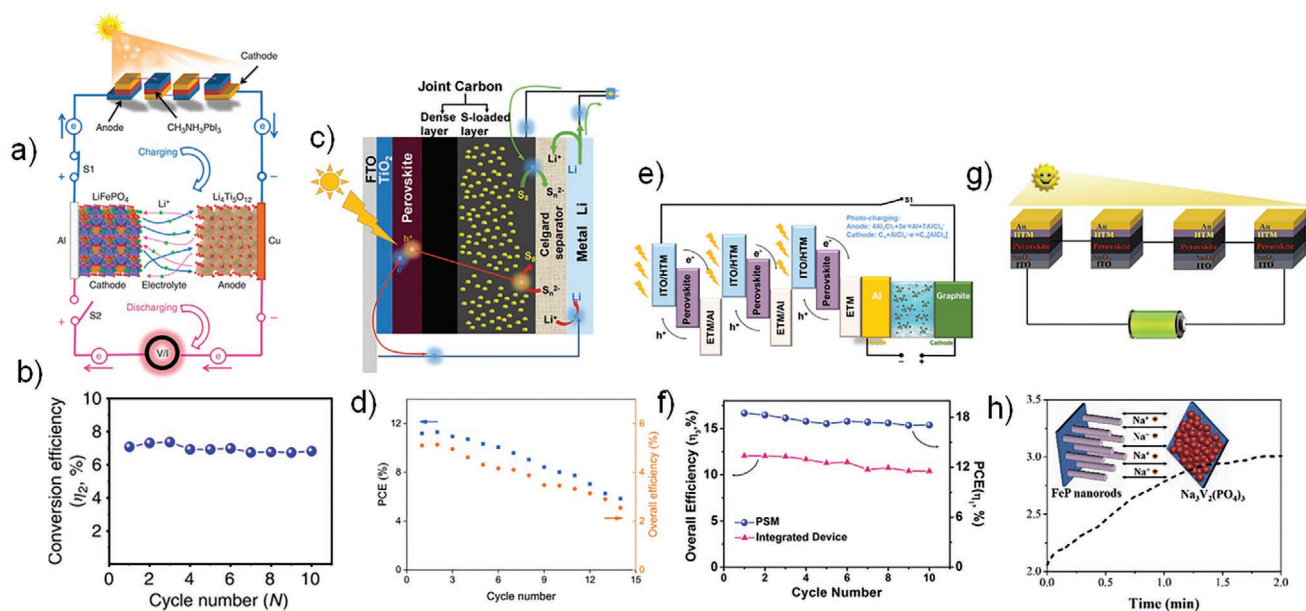


Figure 13. Developed photo-charge batteries. a,b) Integrated solar-rechargeable PSC-lithium-ion battery. Reproduced with permission.^[116] Copyright 2020, Springer Nature. c,d) Integrated solar-rechargeable PSC-lithium-sulfur battery. Reproduced with permission.^[117] Copyright 2019, Wiley. e,f) Integrated solar-rechargeable PSC-aluminum-ion battery. Reproduced with permission.^[118] Copyright 2019, Wiley. g,h) Integrated solar-rechargeable PSC-sodium-ion battery. Reproduced with permission.^[119] Copyright 2019, Elsevier B. V.

Therefore, constructing integrated solar rechargeable batteries is a feasible strategy for energy conversion and storage.

Typically, a full cell of lithium-ion batteries with a low voltage range of 1.0–2.6 V is assembled with LiFePO_4 cathode and $\text{Li}_4\text{Ti}_5\text{O}_{12}$ anode in 1 M LiFP_6 carbonate-based electrolyte^[116] (Figure 13a,b). Four MAPbI_3 solar cells are connected as a power supply unit with high output voltage of 3.84 V. Such structure design can work to directly photo-charge the lithium-ion cell with overall conversion and storage efficiency of 7.80%. Cycling stability is maintained at a high level with the first ten photo-charge and galvanostatic discharge cycles (79.49% initial capacity, $\approx 2.05\%$ decay per cycle). Nevertheless, the long-term operation stability still needs further improvement for potential application.

High-energy lithium–sulfur battery has attracted a lot of attention in recent years, which is also introduced into the photo-charge system by combining three MAPbI_3 solar cells as energy supply unit with efficiency of more than 12% and high V_{OC} of 2.8 V, as depicted in Figure 13c,d.^[117] The integrated solar-driven rechargeable lithium–sulfur battery system is fabricated by joint carbon electrode instead of external wires, indicating an advantage for potential application because of simple structure, and high integration. Moreover, the highest overall energy conversion efficiency of 5.14% can be realized for the integrated device with the specific capacity of 750 mAh g^{-1} . Actually, the photo-charge battery system can be further extended to Al-ion battery^[118] (Figure 13e,f), and Na-ion battery^[119] (Figure 13g,h). The researchers also establish photo-charging battery system by combining wire-connected PSCs unit to obtain high charge voltage.

On this basis, monolithic tandem solar cell, a simple and efficient approach, become the next-generation candidate with higher voltage to supply energy for suitable electrochemical

redox couples. On this basis, rechargeable batteries can store more solar energy as chemical energy, and release the chemical energy as electric energy for supplies. From the perspective of industrialization, 2T-PBTSCs can be used to photo-charge batteries without extra wires. The integrated device is looking forward to further improve the photo-electric conversion and storage efficiency.

4. Summary and Outlook

Tandem solar cells with high voltage and high efficiency have attracted world-wide attention, especially when combined with the efficient PSCs. Herein in this review, we present a practical perspective of high voltage obtained by tandem solar cells, particularly the 2T-PBTSCs. Since voltage is attributed to the energy level of electrons of key storage materials, the high voltage of PSCs and the derived 2T-PBTSCs is of great significance for subsequent application for energy conversion and storage. When applied in hydrogen production by solar water-splitting, CO_2 reduction systems, capacitors, and rechargeable batteries, 2T-PBTSCs could provide high voltage to ensure solar conversion to chemical fuels or chemical energy stored in power sources. We could predict optimistically that those efficient and high-voltage 2T-PBTSCs would play an indispensable role in high efficient energy conversion and storage for future “Internet of Things” society.

Although the 2T-PBTSCs show an encouraging trend on output voltage and efficiency, there are still some key challenges to face in future research: Effective CRL needs to be explored with higher transparency and minimal losses. Stability challenges also remain, such as water, air, temperature, or illumination, especially, long-term stable working voltage.

Meanwhile, the manufacture technique of monolithic interconnection should be promoted for effective 2T-PBTSCs-based integrated devices.

There is no doubt that PSC is a rising star in photovoltaic filed in the past decade with fruitful achievements. The next movement of PSC is definitely toward commercial application, which means higher efficiency, practicability, and low cost. Along with further related researches, we believe highly efficient and low-cost tandem devices could be achieved and 2T-PBTSCs would have broader applications. Some suggestions and perspective are tentatively proposed for the future possible directions:

- 1) Investigation of new materials. In spite of highly efficient PSCs achieved in the past, the key issue of stability will determine whether PSCs could culminate at commercialization, similar to Si-based solar cells. Especially, the resistance toward moisture, oxygen, light, thermal, and mechanical damage would be fateful for the future development of PSCs. Besides, could the toxic Pb be fully replaced by environmental-friendly elements? Those topics call in-depth revolution of new materials for PSCs and PSCs-based tandem devices.
- 2) Development of new technologies. The spin-coating method is still widely used for highly efficient PSCs, which could hardly be applied in industry production. New technologies originated from interdisciplinary technologies, especially semiconductor industry and nanotechnology, should be introduced into PSCs and PSCs-based tandem devices, in order to face the complexity on the working mechanism, key materials, and cell structure.
- 3) Exploration of new mechanisms. Besides the chasing of high efficiency, PSCs-based tandem devices have special advantages in energy conversion/storage. In particular, the integrated devices can be fabricated effectively from SCs-based tandem solar cells as an excitation source unit and energy conversion and storage devices as an application source unit. Herein, new working mechanisms should be explored based on the voltage matching, energy matching, and efficiency matching principles for various energy conversion/storage applications.

Acknowledgements

Financial supports from National Natural Science Foundation (21875123) of China are gratefully acknowledged.

Conflict of Interest

The authors declare no conflict of interest.

Keywords

energy storage, high voltage, perovskite solar cells, solar cells, tandem solar cells

Received: October 2, 2020

Revised: January 23, 2021

Published online:

- [1] W. Wang, X. Xu, W. Zhou, Z. Shao, *Adv. Sci.* **2017**, *4*, 1600371.
- [2] W. Shockley, H. J. Queisser, *J. Appl. Phys.* **1961**, *32*, 510.
- [3] A. D. Vos, *J. Phys. D: Appl. Phys.* **1980**, *13*, 839.
- [4] J. Gobrecht, R. Potter, R. Nottenburg, S. Wagner, *J. Electrochem. Soc.* **1983**, *130*, 2280.
- [5] J. Duan, Y. Zhao, X. Yang, Y. Wang, B. He, Q. Tang, *Adv. Energy Mater.* **2018**, *8*, 1802346.
- [6] Q. Yin, K. Zhang, L. Zhang, J. Jia, X. Zhang, S. Pang, Q.-H. Xu, C. Duan, F. Huang, Y. Cao, *J. Mater. Chem. A* **2019**, *7*, 12426.
- [7] F. Dimroth, T. N. D. Tibbits, M. Niemeier, F. Predan, P. Beutel, C. Karcher, E. Oliva, G. Siefert, D. Lackner, P. Fuschl, A. W. Bett, R. Krause, C. Dräke, E. Guio, J. Wasselin, A. Tauzin, T. Signamarcheix, *IEEE J. Photovoltaics* **2016**, *6*, 343.
- [8] Y. Zhang, Q. Wang, X.-B. Zhang, N. Peng, Z.-Q. Liu, B.-Z. Chen, S.-S. Huang, Z.-Y. Wang, *Chin. Phys. Lett.* **2017**, *34*, 028802.
- [9] J. F. Geisz, M. A. Steiner, N. Jain, K. L. Schulte, R. M. France, W. E. McMahon, E. E. Perl, D. J. Friedman, *IEEE J. Photovoltaics* **2018**, *8*, 626.
- [10] a) R. Isoaho, A. Aho, A. Tukiainen, T. Aho, M. Raappana, T. Salminen, J. Reuna, M. Guina, *Sol. Energy Mater. Sol. Cells* **2019**, *195*, 198; b) I. E. Hashem, C. Zachary Carlin, B. G. Hagar, P. C. Colter, S. M. Bedair, *J. Appl. Phys.* **2016**, *119*, 095706; c) M. Vaisman, K. Mukherjee, T. Masuda, K. Nay Yaung, E. A. Fitzgerald, M. L. Lee, *IEEE J. Photovoltaics* **2016**, *6*, 571; d) Y. Hoshina, M. Shimizu, A. Yamada, M. Konagai, *Jpn. J. Appl. Phys.* **2011**, *50*, 1178; e) B.-Z. Chen, Y. Zhang, Q. Wang, Z.-Y. Wang, *Chin. Phys. Lett.* **2018**, *35*, 078801; f) M. P. Lumb, S. Mack, K. J. Schmieder, M. González, M. F. Bennett, D. Scheiman, M. Meitl, B. Fisher, S. Burroughs, K.-T. Lee, J. A. Rogers, R. J. Walters, *Adv. Energy Mater.* **2017**, *7*, 1700345.
- [11] a) X. Li, W. Zhang, H. Lu, K. Chen, D. Zhou, *J. Cryst. Growth* **2014**, *405*, 16; b) K. L. Schulte, R. M. France, J. F. Geisz, *IEEE J. Photovoltaics* **2017**, *7*, 347.
- [12] A. Kojima, K. Teshima, Y. Shirai, T. Miyasaka, *J. Am. Chem. Soc.* **2009**, *131*, 6050.
- [13] Best Research-Cell Efficiency Chart, <https://www.nrel.gov/pv/cell-efficiency.html> (accessed: January 2021).
- [14] a) G. E. Eperon, S. D. Stranks, C. Menelaou, M. B. Johnston, L. M. Herz, H. J. Snaith, *Energy Environ. Sci.* **2014**, *7*, 982; b) N. Pellet, P. Gao, G. Gregori, T.-Y. Yang, M. K. Nazeeruddin, J. Maier, M. Grätzel, *Angew. Chem.* **2014**, *126*, 3215.
- [15] S. De Wolf, J. Holovsky, S. J. Moon, P. Loper, B. Niesen, M. Ledinsky, F. J. Haug, J. H. Yum, C. Ballif, *J. Phys. Chem. Lett.* **2014**, *5*, 1035.
- [16] Q. Dong, Y. Fang, Y. Shao, P. Mulligan, J. Qiu, L. Cao, J. Huang, *Science* **2015**, *347*, 967.
- [17] a) G. E. Eperon, T. Leijtens, K. A. Bush, R. Prasanna, T. Green, J. T.-W. Wang, D. P. McMeekin, G. Volonakis, R. L. Milot, R. May, A. Palmstrom, D. J. Slotcavage, R. A. Belisle, J. B. Patel, E. S. Parrott, R. J. Sutton, W. Ma, F. Moghadam, B. Conings, A. Babayigit, H.-G. Boyen, S. Bent, F. Giustino, L. M. Herz, M. B. Johnston, M. D. McGehee, H. J. Snaith, *Science* **2016**, *354*, 861; b) F. Hao, C. C. Stoumpos, Z. Liu, R. P. Chang, M. G. Kanatzidis, *J. Am. Chem. Soc.* **2014**, *136*, 16411; c) E. L. Unger, L. Kegelmann, K. Suchan, D. Sörell, L. Korte, S. Albrecht, *J. Mater. Chem. A* **2017**, *5*, 11401; d) F. C. Hanusch, E. Wiesenmayer, E. Mankel, A. Binek, P. Angloher, C. Fraunhofer, N. Giesbrecht, J. M. Feckl, W. Jaegermann, D. Johrendt, T. Bein, P. Docampo, *J. Phys. Chem. Lett.* **2014**, *5*, 2791.
- [18] J. P. Mailoa, C. D. Bailie, E. C. Johlin, E. T. Hoke, A. J. Akey, W. H. Nguyen, M. D. McGehee, T. Buonassisi, *Appl. Phys. Lett.* **2015**, *106*, 121105.
- [19] S. Albrecht, M. Saliba, J. P. Correa Baena, F. Lang, L. Kegelmann, M. Mews, L. Steier, A. Abate, J. Rappich, L. Korte, R. Schlattmann,

- M. K. Nazeeruddin, A. Hagfeldt, M. Grätzel, B. Rech, *Energy Environ. Sci.* **2016**, *9*, 81.
- [20] J. Werner, C. H. Weng, A. Walter, L. Fesquet, J. P. Seif, S. De Wolf, B. Niesen, C. Ballif, *J. Phys. Chem. Lett.* **2016**, *7*, 161.
- [21] J. Werner, L. Barraud, A. Walter, M. Bräuninger, F. Sahli, D. Sacchetto, N. Tétreault, B. Paviet-Salomon, S.-J. Moon, C. Allebé, M. Despeisse, S. Nicolay, S. De Wolf, B. Niesen, C. Ballif, *ACS Energy Lett.* **2016**, *1*, 474.
- [22] J. Werner, A. Walter, E. Rucavado, S.-J. Moon, D. Sacchetto, M. Rienaecker, R. Peibst, R. Brendel, X. Niquille, S. De Wolf, P. Löper, M. Morales-Masis, S. Nicolay, B. Niesen, C. Ballif, *Appl. Phys. Lett.* **2016**, *109*, 233902.
- [23] K. A. Bush, A. F. Palmstrom, Z. J. Yu, M. Boccard, R. Cheacharoen, J. P. Mailoa, D. P. McMeehin, R. L. Z. Hoye, C. D. Bailie, T. Leijtens, I. M. Peters, M. C. Minichetti, N. Rolston, R. Prasanna, S. Sofia, D. Harwood, W. Ma, F. Moghadam, H. J. Snaith, T. Buonassisi, Z. C. Holman, S. F. Bent, M. D. McGehee, *Nat. Energy* **2017**, *2*, 17009.
- [24] Y. Wu, D. Yan, J. Peng, T. Duong, Y. Wan, S. P. Phang, H. Shen, N. Wu, C. Barugkin, X. Fu, S. Surve, D. Grant, D. Walter, T. P. White, K. R. Catchpole, K. J. Weber, *Energy Environ. Sci.* **2017**, *10*, 2472.
- [25] F. Sahli, B. A. Kamino, J. Werner, M. Brauning, B. Paviet-Salomon, L. Barraud, R. Monnard, J. P. Seif, A. Tomasi, Q. Jeangros, A. Hessler-Wyser, S. De Wolf, M. Despeisse, S. Nicolay, B. Niesen, C. Ballif, *Adv. Energy Mater.* **2018**, *8*, 1701609.
- [26] R. Fan, N. Zhou, L. Zhang, R. Yang, Y. Meng, L. Li, T. Guo, Y. Chen, Z. Xu, G. Zheng, Y. Huang, L. Li, L. Qin, X. Qiu, Q. Chen, H. Zhou, *Sol. RRL* **2017**, *1*, 1700149.
- [27] S. Zhu, X. Yao, Q. Ren, C. Zheng, S. Li, Y. Tong, B. Shi, S. Guo, L. Fan, H. Ren, C. Wei, B. Li, Y. Ding, Q. Huang, Y. Li, Y. Zhao, X. Zhang, *Nano Energy* **2018**, *45*, 280.
- [28] Q. Ren, S. Li, S. Zhu, H. Ren, X. Yao, C. Wei, B. Yan, Y. Zhao, X. Zhang, *Sol. Energy Mater. Sol. Cells* **2018**, *185*, 124.
- [29] J. Zheng, C. F. J. Lau, H. Mehrvarz, F.-J. Ma, Y. Jiang, X. Deng, A. Soeriyadi, J. Kim, M. Zhang, L. Hu, X. Cui, D. S. Lee, J. Bing, Y. Cho, C. Chen, M. A. Green, S. Huang, A. W. Y. Ho-Baillie, *Energy Environ. Sci.* **2018**, *11*, 2432.
- [30] F. Sahli, J. Werner, B. A. Kamino, M. Bräuninger, R. Monnard, B. Paviet-Salomon, L. Barraud, L. Ding, J. J. Diaz Leon, D. Sacchetto, G. Cattaneo, M. Despeisse, M. Boccard, S. Nicolay, Q. Jeangros, B. Niesen, C. Ballif, *Nat. Mater.* **2018**, *17*, 820.
- [31] R. L. Z. Hoye, K. A. Bush, F. Oviedo, S. E. Sofia, M. Thway, X. Li, Z. Liu, J. Jean, J. P. Mailoa, A. Oshero, F. Lin, A. F. Palmstrom, V. Bulovic, M. D. McGehee, I. M. Peters, T. Buonassisi, *IEEE J. Photovoltaics* **2018**, *8*, 1023.
- [32] J. Zheng, H. Mehrvarz, F.-J. Ma, C. F. J. Lau, M. A. Green, S. Huang, A. W. Y. Ho-Baillie, *ACS Energy Lett.* **2018**, *3*, 2299.
- [33] K. A. Bush, S. Manzo, K. Frohna, Z. J. Yu, J. A. Raiford, A. F. Palmstrom, H.-P. Wang, R. Prasanna, S. F. Bent, Z. C. Holman, M. D. McGehee, *ACS Energy Lett.* **2018**, *3*, 2173.
- [34] M. Jošt, E. Köhnen, A. B. Morales-Vilches, B. Lipovšek, K. Jäger, B. Macco, A. Al-Ashouri, J. Krč, L. Korte, B. Rech, R. Schlatmann, M. Topič, B. Stannowski, S. Albrecht, *Energy Environ. Sci.* **2018**, *11*, 3511.
- [35] F. Hou, C. Han, O. Isabella, L. Yan, B. Shi, J. Chen, S. An, Z. Zhou, W. Huang, H. Ren, Q. Huang, G. Hou, X. Chen, Y. Li, Y. Ding, G. Wang, C. Wei, D. Zhang, M. Zeman, Y. Zhao, X. Zhang, *Nano Energy* **2019**, *56*, 234.
- [36] H. Shen, S. T. Omelchenko, D. A. Jacobs, S. Yalamanchili, Y. Wan, D. Yan, P. Phang, T. Duong, Y. Wu, Y. Yin, C. Samundsett, J. Peng, N. Wu, T. P. White, G. G. Andersson, N. S. Lewis, K. R. Catchpole, *Sci. Adv.* **2018**, *4*, eaau9711.
- [37] F. Hou, L. Yan, B. Shi, J. Chen, S. Zhu, Q. Ren, S. An, Z. Zhou, H. Ren, C. Wei, Q. Huang, G. Hou, X. Chen, Y. Li, Y. Ding, G. Wang, D. Zhang, Y. Zhao, X. Zhang, *ACS Appl. Energy Mater.* **2019**, *2*, 243.
- [38] B. Chen, Z. Yu, K. Liu, X. Zheng, Y. Liu, J. Shi, D. Spronk, P. N. Rudd, Z. Holman, J. Huang, *Joule* **2019**, *3*, 177.
- [39] L. Mazzarella, Y. H. Lin, S. Kirner, A. B. Morales-Vilches, L. Korte, S. Albrecht, E. Crossland, B. Stannowski, C. Case, H. J. Snaith, R. Schlatmann, *Adv. Energy Mater.* **2019**, *9*, 1803241.
- [40] C. U. Kim, J. C. Yu, E. D. Jung, I. Y. Choi, W. Park, H. Lee, I. Kim, D.-K. Lee, K. K. Hong, M. H. Song, K. J. Choi, *Nano Energy* **2019**, *60*, 213.
- [41] G. Nogay, F. Sahli, J. Werner, R. Monnard, M. Boccard, M. Despeisse, F. J. Haug, Q. Jeangros, A. Ingenito, C. Ballif, *ACS Energy Lett.* **2019**, *4*, 844.
- [42] E. Köhnen, M. Jošt, A. B. Morales-Vilches, P. Tockhorn, A. Al-Ashouri, B. Macco, L. Kegelmann, L. Korte, B. Rech, R. Schlatmann, B. Stannowski, S. Albrecht, *Sustainable Energy Fuels* **2019**, *3*, 1995.
- [43] A. J. Bett, P. S. C. Schulze, K. M. Winkler, Ö. S. Kabakli, I. Ketterer, L. E. Mundt, S. K. Reichmuth, G. Siefer, L. Cojocar, L. Tutsch, M. Bivour, M. Hermle, S. W. Glunz, J. C. Goldschmidt, *Prog. Photovoltaics* **2019**, *28*, 99.
- [44] J. Zheng, H. Mehrvarz, C. Liao, J. Bing, X. Cui, Y. Li, V. R. Gonçalves, C. F. J. Lau, D. S. Lee, Y. Li, M. Zhang, J. Kim, Y. Cho, L. G. Caro, S. Tang, C. Chen, S. Huang, A. W. Y. Ho-Baillie, *ACS Energy Lett.* **2019**, *4*, 2623.
- [45] B. Chen, Z. J. Yu, S. Manzo, S. Wang, W. Weigand, Z. Yu, G. Yang, Z. Ni, X. Dai, Z. C. Holman, J. Huang, *Joule* **2020**, *4*, 850.
- [46] E. Lamanna, F. Matteocci, E. Calabrò, L. Serenelli, E. Salza, L. Martini, F. Menchini, M. Izzì, A. Agresti, S. Pescetelli, S. Bellani, A. E. Del Río Castillo, F. Bonaccorso, M. Tucci, A. Di Carlo, *Joule* **2020**, *4*, 865.
- [47] Y. Hou, E. Aydin, M. De Bastiani, C. Xiao, F. H. Isikgor, D.-J. Xue, B. Chen, H. Chen, B. Bahrami, A. H. Chowdhury, A. Johnston, S.-W. Baek, Z. Huang, M. Wei, Y. Dong, J. Troughton, R. Jalmo, A. J. Mirabelli, T. G. Allen, E. Van Kerschaver, M. I. Saidaminov, D. Baran, Q. Qiao, K. Zhu, S. De Wolf, E. H. Sargent, *Science* **2020**, *367*, 1135.
- [48] D. Kim, H. J. Jung, I. J. Park, B. W. Larson, S. P. Dunfield, C. Xiao, J. Kim, J. Tong, P. Boonmongkolras, S. G. Ji, F. Zhang, S. R. Pae, M. Kim, S. B. Kang, V. Dravid, J. J. Berry, J. Y. Kim, K. Zhu, D. H. Kim, B. Shin, *Science* **2020**, *368*, 155.
- [49] P. S. C. Schulze, A. J. Bett, M. Bivour, P. Caprioglio, F. M. Gerspacher, Ö. Ş. Kabaklı, A. Richter, M. Stolterfoht, Q. Zhang, D. Neher, M. Hermle, H. Hillebrecht, S. W. Glunz, J. C. Goldschmidt, *Sol. RRL* **2020**, *4*, 2000152.
- [50] A. Al-Ashouri, E. Köhnen, B. Li, A. Magomedov, H. Hempel, P. Caprioglio, J. A. Marquez, A. B. Morales Vilches, E. Kasparavicius, J. A. Smith, N. Phung, D. Menzel, M. Grischek, L. Kegelmann, D. Skroblin, C. Gollwitzer, T. Malinauskas, M. Jost, G. Matic, B. Rech, R. Schlatmann, M. Topic, L. Korte, A. Abate, B. Stannowski, D. Neher, M. Stolterfoht, T. Unold, V. Getautis, S. Albrecht, *Science* **2020**, *370*, 1300.
- [51] K. Yoshikawa, W. Yoshida, T. Irie, H. Kawasaki, K. Konishi, H. Ishibashi, T. Asatani, D. Adachi, M. Kanematsu, H. Uzu, K. Yamamoto, *Sol. Energy Mater. Sol. Cells* **2017**, *173*, 37.
- [52] A. Richter, M. Hermle, S. W. Glunz, *IEEE J. Photovoltaics* **2013**, *3*, 1184.
- [53] C. D. Bailie, M. G. Christoforo, J. P. Mailoa, A. R. Bowring, E. L. Unger, W. H. Nguyen, J. Burschka, N. Pellet, J. Z. Lee, M. Grätzel, R. Noufi, T. Buonassisi, A. Salleo, M. D. McGehee, *Energy Environ. Sci.* **2015**, *8*, 956.
- [54] M. Taguchi, A. Yano, S. Tohoda, K. Matsuyama, Y. Nakamura, T. Nishiwaki, K. Fujita, E. Maruyama, *IEEE J. Photovoltaics* **2014**, *4*, 96.

- [55] C. Ulbrich, A. Gerber, K. Hermans, A. Lambertz, U. Rau, *Prog. Photovoltaics* **2013**, *21*, 1672.
- [56] H. Kanda, N. Shibayama, A. Uzum, T. Umeyama, H. Imahori, K. Ibi, S. Ito, *ACS Appl. Mater. Interfaces* **2018**, *10*, 35016.
- [57] S. M. Iftiqar, J. Jung, J. Yi, *J. Phys. D: Appl. Phys.* **2017**, *50*, 405501.
- [58] a) R. E. Beal, D. J. Slotcavage, T. Leijtens, A. R. Bowring, R. A. Belisle, W. H. Nguyen, G. F. Burkhard, E. T. Hoke, M. D. McGehee, *J. Phys. Chem. Lett.* **2016**, *7*, 746; b) Y. Zhou, F. Wang, Y. Cao, J.-P. Wang, H.-H. Fang, M. A. Loi, N. Zhao, C.-P. Wong, *Adv. Energy Mater.* **2017**, *7*, 1701048; c) J. K. Kim, S. U. Chai, Y. Ji, B. Levy-Wendt, S. H. Kim, Y. Yi, T. F. Heinz, J. K. Nørskov, J. H. Park, X. Zheng, *Adv. Energy Mater.* **2018**, *8*, 1801717.
- [59] S. Albrecht, M. Saliba, J.-P. Correa-Baena, K. Jäger, L. Korte, A. Hagfeldt, M. Grätzel, B. Rech, *J. Opt.* **2016**, *18*, 064012.
- [60] a) J.-W. Lee, D.-H. Kim, H.-S. Kim, S.-W. Seo, S. M. Cho, N.-G. Park, *Adv. Energy Mater.* **2015**, *5*, 1501310; b) C. Yi, J. Luo, S. Meloni, A. Boziki, N. Ashari-Astani, C. Grätzel, S. M. Zakeeruddin, U. Röthlisberger, M. Grätzel, *Energy Environ. Sci.* **2016**, *9*, 656; c) X. Xia, W. Wu, H. Li, B. Zheng, Y. Xue, J. Xu, D. Zhang, C. Gao, X. Liu, *RSC Adv.* **2016**, *6*, 14792; d) D. P. McMeekin, G. Sadoughi, W. Rehman, G. E. Eperon, M. Saliba, M. T. Hörlantner, A. Haghighirad, N. Sakai, L. Korte, B. Rech, M. B. Johnston, L. M. Herz, H. J. Snaith, *Science* **2016**, *351*, 151; e) M. Saliba, T. Matsui, J. Y. Seo, K. Domanski, J. P. Correa-Baena, M. K. Nazeeruddin, S. M. Zakeeruddin, W. Tress, A. Abate, A. Hagfeldt, M. Grätzel, *Energy Environ. Sci.* **2016**, *9*, 1989.
- [61] F. Sahli, J. Werner, B. A. Kamino, M. Brauning, R. Monnard, B. Paviat-Salomon, L. Barraud, L. Ding, J. J. Diaz Leon, D. Sacchetto, G. Cattaneo, M. Despeisse, M. Boccard, S. Nicolay, Q. Jeangros, B. Niesen, C. Ballif, *Nat. Mater.* **2018**, *17*, 820.
- [62] A. S. Subbiah, F. H. Isikgor, C. T. Howells, M. De Bastiani, J. Liu, E. Aydin, F. Furlan, T. G. Allen, F. Xu, S. Zhumagali, S. Hoogland, E. H. Sargent, I. McCulloch, S. De Wolf, *ACS Energy Lett.* **2020**, *5*, 3034.
- [63] J. Ávila, C. Momblona, P. Boix, M. Sessolo, M. Anaya, G. Lozano, K. Vandewal, H. Míguez, H. J. Bolink, *Energy Environ. Sci.* **2018**, *11*, 3292.
- [64] F. Jiang, T. Liu, B. Luo, J. Tong, F. Qin, S. Xiong, Z. Li, Y. Zhou, *J. Mater. Chem. A* **2016**, *4*, 1208.
- [65] D. Forgács, L. Gil-Escrig, D. Pérez-Del-Rey, C. Momblona, J. Werner, B. Niesen, C. Ballif, M. Sessolo, H. J. Bolink, *Adv. Energy Mater.* **2017**, *7*, 1602121.
- [66] Z. Yang, Z. Yu, H. Wei, X. Xiao, Z. Ni, B. Chen, Y. Deng, S. N. Habisreutinger, X. Chen, K. Wang, J. Zhao, P. N. Rudd, J. J. Berry, M. C. Beard, J. Huang, *Nat. Commun.* **2019**, *10*, 4498.
- [67] R. Lin, K. Xiao, Z. Qin, Q. Han, C. Zhang, M. Wei, M. I. Saidaminov, Y. Gao, J. Xu, M. Xiao, A. Li, J. Zhu, E. H. Sargent, H. Tan, *Nat. Energy* **2019**, *4*, 864.
- [68] C. Li, Z. S. Wang, H. L. Zhu, D. Zhang, J. Cheng, H. Lin, D. Ouyang, W. C. H. Choy, *Adv. Energy Mater.* **2018**, *8*, 1801954.
- [69] a) A. Rajagopal, Z. Yang, S. B. Jo, I. L. Braly, P. W. Liang, H. W. Hillhouse, A. K. Jen, *Adv. Mater.* **2017**, *29*, 1702140; b) T. Leijtens, R. Prasanna, K. A. Bush, G. E. Eperon, J. A. Raiford, A. Gold-Parker, E. J. Wolf, S. A. Swifter, C. C. Boyd, H.-P. Wang, M. F. Toney, S. F. Bent, M. D. McGehee, *Sustainable Energy Fuels* **2018**, *2*, 2450.
- [70] D. P. McMeekin, S. Mahesh, N. K. Noel, M. T. Klug, J. Lim, J. H. Warby, J. M. Ball, L. M. Herz, M. B. Johnston, H. J. Snaith, *Joule* **2019**, *3*, 387.
- [71] K. Xiao, R. Lin, Q. Han, Y. Hou, Z. Qin, H. T. Nguyen, J. Wen, M. Wei, V. Yeddu, M. I. Saidaminov, Y. Gao, X. Luo, Y. Wang, H. Gao, C. Zhang, J. Xu, J. Zhu, E. H. Sargent, H. Tan, *Nat. Energy* **2020**, *5*, 870.
- [72] Z. Yu, Z. Yang, Z. Ni, Y. Shao, B. Chen, Y. Lin, H. Wei, Z. J. Yu, Z. Holman, J. Huang, *Nat. Energy* **2020**, *5*, 657.
- [73] S. G. Motti, D. Meggiolaro, A. J. Barker, E. Mosconi, C. A. R. Perini, J. M. Ball, M. Gandini, M. Kim, F. De Angelis, A. Petrozza, *Nat. Photonics* **2019**, *13*, 532.
- [74] R. Sheng, M. T. Hörlantner, Z. Wang, Y. Jiang, W. Zhang, A. Agosti, S. Huang, X. Hao, A. Ho-Baillie, M. Green, H. J. Snaith, *J. Phys. Chem. C* **2017**, *121*, 27256.
- [75] C.-Y. Chang, B.-C. Tsai, Y.-C. Hsiao, M.-Z. Lin, H.-F. Meng, *Nano Energy* **2019**, *55*, 354.
- [76] J. Tong, Z. Song, D. H. Kim, X. Chen, C. Chen, A. F. Palmstrom, P. F. Ndione, M. O. Reese, S. P. Dunfield, O. G. Reid, J. Liu, F. Zhang, S. P. Harvey, Z. Li, S. T. Christensen, G. Teeter, D. Zhao, M. M. Al-Jassim, M. F. A. M. van Hest, M. C. Beard, S. E. Shaheen, J. J. Berry, Y. Yan, K. Zhu, *Science* **2019**, *364*, 475.
- [77] M. Wei, K. Xiao, G. Walters, R. Lin, Y. Zhao, M. I. Saidaminov, P. Todorovic, A. Johnston, Z. Huang, H. Chen, A. Li, J. Zhu, Z. Yang, Y. K. Wang, A. H. Proppe, S. O. Kelley, Y. Hou, O. Voznyy, H. Tan, E. H. Sargent, *Adv. Mater.* **2020**, *32*, 1907058.
- [78] D. Zhao, C. Chen, C. Wang, M. M. Junda, Z. Song, C. R. Grice, Y. Yu, C. Li, B. Subedi, N. J. Podraza, X. Zhao, G. Fang, R.-G. Xiong, K. Zhu, Y. Yan, *Nat. Energy* **2018**, *3*, 1093.
- [79] A. F. Palmstrom, G. E. Eperon, T. Leijtens, R. Prasanna, S. N. Habisreutinger, W. Nemeth, E. A. Gaulding, S. P. Dunfield, M. Reese, S. Nanayakkara, T. Moot, J. Werner, J. Liu, B. To, S. T. Christensen, M. D. McGehee, M. F. A. M. van Hest, J. M. Luther, J. J. Berry, D. T. Moore, *Joule* **2019**, *3*, 2193.
- [80] C. Li, Z. Song, C. Chen, C. Xiao, B. Subedi, S. P. Harvey, N. Shrestha, K. K. Subedi, L. Chen, D. Liu, Y. Li, Y.-W. Kim, C.-s. Jiang, M. J. Heben, D. Zhao, R. J. Ellingson, N. J. Podraza, M. Al-Jassim, Y. Yan, *Nat. Energy* **2020**, *5*, 768.
- [81] Y. Tong, Z. Xiao, X. Du, C. Zuo, Y. Li, M. Lv, Y. Yuan, C. Yi, F. Hao, Y. Hua, T. Lei, Q. Lin, K. Sun, D. Zhao, C. Duan, X. Shao, W. Li, H.-L. Yip, Z. Xiao, B. Zhang, Q. Bian, Y. Cheng, S. Liu, M. Cheng, Z. Jin, S. Yang, L. Ding, *Sci. China: Chem.* **2020**, *63*, 758.
- [82] a) X. Xu, K. Feng, Z. Bi, W. Ma, G. Zhang, Q. Peng, *Adv. Mater.* **2019**, *31*, 1901872; b) J. Yuan, Y. Zhang, L. Zhou, G. Zhang, H.-L. Yip, T.-K. Lau, X. Lu, C. Zhu, H. Peng, P. A. Johnson, M. Leclerc, Y. Cao, J. Ulanski, Y. Li, Y. Zou, *Joule* **2019**, *3*, 1140.
- [83] L. Dou, Y. Liu, Z. Hong, G. Li, Y. Yang, *Chem. Rev.* **2015**, *115*, 12633.
- [84] C.-C. Chen, S.-H. Bae, W.-H. Chang, Z. Hong, G. Li, Q. Chen, H. Zhou, Y. Yang, *Mater. Horiz.* **2015**, *2*, 203.
- [85] Y. Liu, L. A. Renne, M. Bag, Z. A. Page, P. Kim, J. Choi, T. Emrick, D. Venkataraman, T. P. Russell, *ACS Appl. Mater. Interfaces* **2016**, *8*, 7070.
- [86] Z. Li, S. Wu, J. Zhang, K. C. Lee, H. Lei, F. Lin, Z. Wang, Z. Zhu, A. K. Y. Jen, *Adv. Energy Mater.* **2020**, *10*, 2000361.
- [87] J. Liu, S. Lu, L. Zhu, X. Li, W. C. Choy, *Nanoscale* **2016**, *8*, 3638.
- [88] Q. Zeng, L. Liu, Z. Xiao, F. Liu, Y. Hua, Y. Yuan, L. Ding, *Sci. Bull.* **2019**, *64*, 885.
- [89] X. Chen, Z. Jia, Z. Chen, T. Jiang, L. Bai, F. Tao, J. Chen, X. Chen, T. Liu, X. Xu, C. Yang, W. Shen, W. E. I. Sha, H. Zhu, Y. Yang, *Joule* **2020**, *4*, 1.
- [90] S. Xie, R. Xia, Z. Chen, J. Tian, L. Yan, M. Ren, Z. Li, G. Zhang, Q. Xue, H.-L. Yip, Y. Cao, *Nano Energy* **2020**, *78*, 105238.
- [91] a) T. Feurer, B. Bissig, T. P. Weiss, R. Carron, E. Avancini, J. Lockinger, S. Buecheler, A. N. Tiwari, *Sci. Technol. Adv. Mater.* **2018**, *19*, 263; b) H. Elanzeery, F. Babbe, M. Melchiorre, A. Zelenina, S. Siebentritt, *IEEE J. Photovoltaics* **2017**, *7*, 684; c) K. Kim, S. K. Ahn, J. H. Choi, J. Yoo, Y.-J. Eo, J.-S. Cho, A. Cho, J. Gwak, S. Song, D.-H. Cho, Y.-D. Chung, J. H. Yun, *Nano Energy* **2018**, *48*, 345; d) M. Topic, R. M. Geisthardt, J. R. Sites, *IEEE J. Photovoltaics* **2015**, *5*, 360; e) T. K. Todorov, O. Gunawan, T. Gokmen, D. B. Mitzi, *Prog. Photovoltaics* **2013**, *21*, 82.

- [92] T. Todorov, T. Gershon, O. Gunawan, Y. S. Lee, C. Sturdevant, L.-Y. Chang, S. Guha, *Adv. Energy Mater.* **2015**, 5, 1500799.
- [93] Y. H. Jang, J. M. Lee, J. W. Seo, I. Kim, D.-K. Lee, *J. Mater. Chem. A* **2017**, 5, 19439.
- [94] Q. Han, Y.-T. Hsieh, L. Meng, J.-L. Wu, P. Sun, E.-P. Yao, S.-Y. Chang, S.-H. Bae, T. Kato, V. Bermudez, Y. Yang, *Science* **2018**, 361, 904.
- [95] M. Jošt, T. Bertram, D. Koushik, J. A. Marquez, M. A. Verheijen, M. D. Heinemann, E. Köhnen, A. Al-Ashouri, S. Braunger, F. Lang, B. Rech, T. Unold, M. Creatore, I. Lauermann, C. A. Kaufmann, R. Schlattmann, S. Albrecht, *ACS Energy Lett.* **2019**, 4, 583.
- [96] A. R. Uhl, Z. Yang, A. K. Y. Jen, H. W. Hillhouse, *J. Mater. Chem. A* **2017**, 5, 3214.
- [97] B. Chen, X. Zheng, Y. Bai, N. P. Padture, J. Huang, *Adv. Energy Mater.* **2017**, 7, 1602400.
- [98] P. Chen, T.-T. Li, G.-R. Li, X.-P. Gao, *Sci. China Mater.* **2020**, 63, 1693.
- [99] a) X. Xu, S. Li, H. Zhang, Y. Shen, S. M. Zakeeruddin, M. Grätzel, Y.-B. Cheng, M. Wang, *ACS Nano* **2015**, 9, 1782; b) P. Du, X. Hu, C. Yi, H. C. Liu, P. Liu, H.-L. Zhang, X. Gong, *Adv. Funct. Mater.* **2015**, 25, 2420.
- [100] J. Xu, Z. Ku, Y. Zhang, D. Chao, H. J. Fan, *Adv. Mater. Technol.* **2016**, 1, 1600074.
- [101] F. Zhou, Z. Ren, Y. Zhao, X. Shen, A. Wang, Y. Y. Li, C. Surya, Y. Chai, *ACS Nano* **2016**, 10, 5900.
- [102] J. Kim, S. M. Lee, Y.-H. Hwang, S. Lee, B. Park, J.-H. Jang, K. Lee, *J. Mater. Chem. A* **2017**, 5, 1906.
- [103] R. Liu, C. Liu, S. Fan, *J. Mater. Chem. A* **2017**, 5, 23078.
- [104] a) J. Liang, G. Zhu, Z. Lu, P. Zhao, C. Wang, Y. Ma, Z. Xu, Y. Wang, Y. Hu, L. Ma, T. Chen, Z. Tie, J. Liu, Z. Jin, *J. Mater. Chem. A* **2018**, 6, 2047; b) J. Liang, G. Zhu, C. Wang, P. Zhao, Y. Wang, Y. Hu, L. Ma, Z. Tie, J. Liu, Z. Jin, *Nano Energy* **2018**, 52, 239.
- [105] Z. Liu, Y. Zhong, B. Sun, X. Liu, J. Han, T. Shi, Z. Tang, G. Liao, *ACS Appl. Mater. Interfaces* **2017**, 9, 22361.
- [106] F. Zhang, W. Li, Z. Xu, M. Ye, H. Xu, W. Guo, X. Liu, *Nano Energy* **2018**, 46, 168.
- [107] A. R. Bin, M. Yusoff, J. Jang, *Chem. Commun.* **2016**, 52, 5824.
- [108] J. Luo, J. H. Im, M. T. Mayer, M. Schreier, M. K. Nazeeruddin, N. G. Park, S. D. Tilley, H. J. Fan, M. Grätzel, *Science* **2014**, 345, 1593.
- [109] R. E. Rocheleau, E. L. Miller, A. Misra, *Energy Fuels* **1998**, 12, 3.
- [110] O. Khaselev, J. A. Turner, *Science* **1998**, 280, 425.
- [111] G. Gurudayal, J. W. Beeman, J. Bullock, H. Wang, J. Eichhorn, C. Towle, A. Javey, F. M. Toma, N. Mathews, J. W. Ager, *Energy Environ. Sci.* **2019**, 12, 1068.
- [112] M. Schreier, L. Curvat, F. Giordano, L. Steier, A. Abate, S. M. Zakeeruddin, J. Luo, M. T. Mayer, M. Grätzel, *Nat. Commun.* **2015**, 6, 7326.
- [113] Y. Mi, Y. Qiu, Y. Liu, X. Peng, M. Hu, S. Zhao, H. Cao, L. Zhuo, H. Li, J. Ren, X. Liu, J. Luo, *Adv. Funct. Mater.* **2020**, 30, 2003438.
- [114] K. Xiao, J. Wen, Q. Han, R. Lin, Y. Gao, S. Gu, Y. Zang, Y. Nie, J. Zhu, J. Xu, H. Tan, *ACS Energy Lett.* **2020**, 5, 2819.
- [115] J. Wang, V. Zardetto, K. Datta, D. Zhang, M. M. Wienk, R. A. J. Janssen, *Nat. Commun.* **2020**, 11, 5254.
- [116] J. Xu, Y. Chen, L. Dai, *Nat. Commun.* **2015**, 6, 8103.
- [117] P. Chen, G. R. Li, T. T. Li, X. P. Gao, *Adv. Sci.* **2019**, 6, 1900620.
- [118] Y. Hu, Y. Bai, B. Luo, S. Wang, H. Hu, P. Chen, M. Lyu, J. Shapter, A. Rowan, L. Wang, *Adv. Energy Mater.* **2019**, 9, 1900872.
- [119] L. Wang, X. Zhao, S. Dai, Y. Shen, M. Wang, *Electrochim. Acta* **2019**, 314, 142.



Tian-Tian Li is a Ph.D. candidate in the School of Materials Science and Engineering, Nankai University. She received her Bachelor of Engineering degree in 2017 from the School of Materials Science and Engineering, Yanshan University of China. Her general research interests are in the area of perovskite tandem solar cells and novel solar energy conversion and storage systems.



Yuan-Bo Yang is a Ph.D. candidate in the School of Materials Science and Engineering, Nankai University. He received his M.S. in 2018 from the School of Materials Science and Engineering, China University of Mining and Technology. He has focused his research on perovskite solar cells with a special interest in electron transport layers and carbon-based HTM-free structures.



Guo-Ran Li is a full professor in Institute of New Energy Material Chemistry, Nankai University. His main current research interest is study on functional materials for new energy, and in particular for hybrid solar cells and rechargeable batteries. Guo-ran received a Bachelor degree in Chemistry and a Ph.D. degree in Physical Chemistry from Nankai University, respectively, in 2000 and 2005. He worked in Queensland University of Technology as an Endeavour Research Fellow in 2008, and as a visiting professor in Department of Materials Science and Metallurgy, University of Cambridge from 2014 to 2015.



Peng Chen is a lecturer in School of Materials Science and Engineering, Nankai University. He received his B.S. degree in 2015 from College of Chemistry and Ph.D. degree in 2020 from School of Materials Science and Engineering, Nankai University of China, respectively. His general research interests are in the area of novel energy conversion and storage systems including solar rechargeable batteries, new type solar cells, and all-solid batteries.



Xue-Ping Gao is professor in Institute of New Energy Material Chemistry, Nankai University of China. He received his doctorate at Department of Chemistry from Nankai University in 1995. He used to work as a visiting research fellow at Kogakuin University in Japan from 1997 to 1999. Currently, his main research is focused on energy storage materials for power sources, including Li-ion batteries, Li-S battery, and solar rechargeable battery.